A human retinal microvascular endothelial-pericyte co-culture model to study diabetic retinopathy in vitro

Jessica J. Eyre, Rachel L. Williams & Hannah J. Levis

Department of Eye and Vision Science, Institute of Life Course & Medical Sciences, University of Liverpool, William Henry Duncan Building, 6 West Derby St, Liverpool, United Kingdom.

ORCID IDs: https://orcid.org/0000-0002-4211-6680, https://orcid.org/ 0000-0002-1954-0256, https://orcid.org/0000-0002-3923-1178

Corresponding author: Jessica J Eyre

Email: jjeyre@liverpool.ac.uk

Tel: 0151 7949034

Address: First Floor, William Henry Duncan Building, 6 West Derby St, Liverpool, L7 8TX, United Kingdom.

Co-Authors: rlw@liverpool.ac.uk, h.levis@liverpool.ac.uk

The authors declare no conflict of interests

[1]

[1] **Abbreviations**

αSMA- alpha-smooth muscle actin, Ang-2- angiopoietin-2, BRB- blood-retinal-barrier, Cx43- connexin-43, DAPI- 4′,6-diamidino-2-phenylindole, DR- diabetic retinopathy, EC- endothelial cell, ECM- extracellular matrix, F-actin- filamentous actin , FBS- foetal bovine serum, GJ- gap junctions, hHGF- human hepatocyte growth factor, H- hour, hREC- human retinal microvascular endothelial cell, hRP- human retinal pericyte , IF- immunofluorescence, IL-8- interleukin-8, PET- polyethylene terephthalate, PDGF- platelet-derived growth factor, REC- retinal endothelial cell, RP- retinal pericyte, RT- room temperature, SD- standard deviation TC- tissue culture, TJ- tight junction, TIMP-2- tissue inhibitor for metalloproteinase-2, VE-Cad- vascular endothelial cadherin, VEGF- vascular endothelial growth factor, ZO-1- zonula occludens-1

Abstract

This human primary co-culture model using human retinal microvascular endothelial cells (hREC) and human retinal pericyte cells (hRP) aims to improve current understanding of the cellular changes occurring in the retinal microvasculature during diabetic retinopathy (DR). Currently, patients often present in clinic with late-stage DR, only when vision becomes impaired. Therefore, new strategies for earlier detection in clinic, combined with novel pharmaceutical and cellular interventions are essential in order to slow or halt the progression of DR from background to sight-threatening stage. This co-culture model can be used as a simple, replicable in vitro tool to discover and assess novel drug therapies and improve fundamental understanding of alterations to cell behaviour in the human retinal microvasculature during DR.

hRP and hREC were cultured for up to 21 days in normoxic (20%) or hypoxic (2%) oxygen levels and physiological (5.5mM) or very high (33mM) glucose, to maintain a healthy, or induce a diabetic-like phenotype in vitro. Mono- or co-cultured hREC and hRP were seeded 1:1 in healthy (20% oxygen and 5.5mM glucose) or diabetic-like (2% oxygen and 33mM glucose) conditions, on either side of untreated polyethylene terephthalate (PET) transwell inserts, and cultured for 21 days. Mono- and co-cultures were analysed for changes in metabolic activity, angiogenic response and junctional protein expression, using immunofluorescence antibody labelling, flow cytometry and multiplex ELISA technology.

hRP and hREC were successfully co-cultured, and the glucose and oxygen concentrations selected for the in vitro healthy and diabetic-like conditions were sufficient for cell viability and EC monolayer integrity, with evidence of an angiogenic response in diabetic-like conditions within the 21 day timeframe. Angiopoietin-2 (Ang-2), vascular endothelial growth factor (VEGF), and platelet-derived growth factor (PDGF) secretion were all increased, whilst hepatocyte growth factor (hHGF), tissue inhibitor for metalloproteinase-2 (TIMP-2) and interleukin-8 (IL-8) secretion were all reduced in the in vitro diabetic-like conditions. The secretion profile of co-cultures was different to mono-cultures, highlighting the importance of using co-culture models to collect data more reflective of the close relationship between hRP-hREC in vivo.

Previous groups have developed useful co-culture models utilising non-human, immortalised or large vessel-sourced cells to explore changes to the vasculature during hypoxia and/or high glucose insult. In this study the use of human primary, retina-specific microvascular cells, mono- and co-cultured, collected over a longer culture period, has enabled detection of changes that may have been missed in previous models.

Keywords

Angiogenesis, blood-retinal-barrier, co-culture, diabetic retinopathy, endothelial, microvasculature, pericyte

Funding

This study was funded by the Crossley Barnes Bequest Studentship, University of Liverpool.

Graphical Abstract

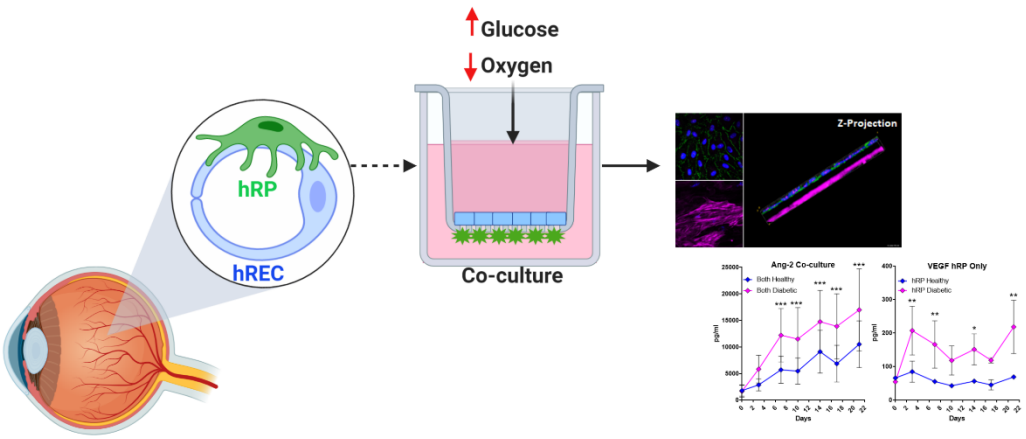

1. Introduction

Diabetic retinopathy (DR) is a major microvascular complication of type 2 diabetes mellitus and leads to vision impairment in >10% of the type 2 diabetes population, equating to >45million people worldwide in 2015 (Yau et al., 2012). Vision-threatening DR is predicted to rise to >70 million people worldwide by 2040, resulting in major economic implications for health services and increased morbidity for people diagnosed with DR (Antonetti et al., 2004; Wild et al., 2004). Deeper understanding of the different stages of cellular change in the retinal capillary microenvironment could lead to novel, early-stage interventions, aimed at preventing vision loss.

The current treatments of anti-vascular endothelial growth factor (VEGF) injections, which can be combined with laser therapy, are only offered at late-stage, once substantial damage has already occurred to the retinal capillaries (Medina et al., 2013). Development of early-stage therapies, which slow or prevent progression, are the ultimate goal. Unravelling the multifactorial aspects of the diabetic milieu, including chronic hyperglycaemia, metabolic dysregulation and ultimately tissue hypoxia, will aid in developing novel therapeutic targets.

The retinal capillaries are composed of an inner layer of microvascular retinal endothelial cells (REC) with tight cell-cell contacts, forming the inner blood-retinal-barrier (BRB), and perivascular retinal pericytes (RP), which wrap around the endothelial cells (EC) providing structural and signalling support. This configuration enables the tightly regulated passage of substances from the blood, to the surrounding highly metabolically active tissue and vice versa. Loss of highly regulated EC-EC contacts, which in healthy conditions are formed by tight junctions (TJ), adherens junctions and gap junctions (GJ), is a major contributor to retinal capillary dysfunction and ultimately breakdown of the BRB. Structurally, basement membrane thickening and pericyte drop-out are early characteristics of DR, where disruption of both structural and cell signalling support from the RP is implicated in EC dysfunction and disease progression (Motiejunaite and Kazlauskas, 2008). However, the chronology of the alterations to cell signalling pathways, BRB breakdown, extracellular matrix (ECM) remodelling and cell death is not fully understood**.**

VEGF and angiopoietin-2 (Ang-2) have major implications in DR progression, due to their involvement in driving the angiogenic switch from non-proliferative to the proliferative-stage (Stitt et al., 2016; Yao et al., 2007). The secretion profile of VEGF, Ang-2, and several other proteins involved in oxidative stress, angiogenesis and hyperglycaemia, is cell-type specific, therefore it is important to co-culture the cells comprising the microvasculature in vitro, in order to ascertain the most relevant cellular changes when modelling DR.

Previously, large vessel-derived, mixed human/animal and immortalised cell co-culture models have been developed, to understand the complex EC:pericyte relationship in blood vessels (Kumar et al., 2011; Tarallo et al., 2012a; Walshe et al., 2011; Wisniewska- Kruk et al., 2012). Both hypoxia and hyperglycaemia are conditions encountered by the cells of the retinal

microvasculature at various stages throughout the progression of DR. To induce a diabetic-like phenotype in vitro, high glucose (33mM) and low oxygen (2%) can be used to accelerate the disease process, which often takes decades in humans. Although ECs in vivo are unlikely to experience simultaneous high glucose and low oxygen, metabolic memory is an important factor of the disease process (Kowluru et al., 2010), characterised by the imprinted effect of high glucose leading to a resistance in the halting of pathology even after restoration of glycaemic control. Using high glucose aims to induce and maintain the diabetic-like hyperglycaemic phenotype over time in vitro, whilst hypoxia aims to induce the oxidative stress ECs may encounter as blood vessel integrity begins to fail in the retinal microvasculature. The current study sought to develop a human, microvascular, in vitro co-culture model using commercially available human RP (hRP) and human REC (hREC). This is a novel, species and tissue-specific, reproducible co-culture model that can be used to study cellular changes, importantly over an extended period of time, as well as providing a potential tool to test novel DR-targeted therapies in vitro.

2. Materials and Methods

2.1 Cell culture

hREC (Cell Systems, Kirkland, WA, USA, ACBRI 181V) were used in experiments up to P10, cultured in PromoCell MV medium (PromoCell, Heidelberg, Germany) containing 5% foetal bovine serum (FBS), further supplemented with heat inactivated FBS (Labtech, East Sussex, UK) to final concentration of 10%. hREC were sub-cultured using 1X Trypsin-EDTA (Sigma, Dorset, UK) at ~90% confluence. hRP (Cell Systems, ACBRI 183V) were used in experiments up to P10, cultured in DMEM (Life Technologies, Warrington, UK) supplemented with 1mM sodium pyruvate (Life Technologies), physiological (5.5mM) [D+] glucose (Life Technologies) and 10% FBS. hRP were sub-cultured at 70-80% confluence using 1X Trypsin-EDTA. To maintain cells with a physiologically healthy phenotype, cells were cultured in 20% oxygen and 5.5mM glucose. High glucose (33mM) was added to create a hyperglycaemic environment, in order to induce a diabetic-like phenotype in vitro. Hypoxic (2% oxygen) insult was used simultaneously to induce an oxidative stress response in the hREC and hRP, which may be encountered by the cells comprising the retinal microvasculature as vessels regress or become unstable as DR progresses.

2.2 Immunocytochemical staining

Cells were fixed for 9 mins using 10% neutral buffered formalin (Sigma), at room temperature (RT). Cells were permeabilised using 0.5% Triton-X (Sigma) for 4 mins. Cells were blocked using 5% normal goat serum (Sigma) for 1 hour (H), at RT. Primary antibodies, (Table 1) were incubated overnight at 4°C. Secondary antibodies (Thermofisher, Waltham, MA, USA) were added at 5µg/ml for 45 mins at RT; goat anti-rabbit-488 and goat anti-mouse-594. For filamentous actin (F-actin) labelling, phalloidin-647 (Thermofisher) was used at 0.22µM and added with the secondary antibodies. Cells were washed in 0.1% Tween-20, then incubated with 300nM 4′,6-diamidino-2-phenylindole (DAPI; Life Technologies) for 20 mins. After a final wash with ddH_2O, hardset mounting media (Agilent, Cheshire, UK) and a cover slip were added.

2.3 Flow cytometry

$1x10^5$ cells/tube were re-suspended in 100µl FACS buffer (dPBS +1% FBS). Fluorescent conjugated antibodies were added at 5µl/tube, or 6µl/tube for anti-CD34 (Table 2). Antibodies were incubated with cells at 4°C for 30 mins then washed in FACS buffer, supernatant removed and the cell pellet resuspended in 300µl fresh FACS buffer. Flow cytometry was performed using a BD Accuri-6 machine and Accuri-C6 software. Flow parameters were $1x10^4$ events, on slow fluidics. Un-labelled cells were used to exclude dead cells/debris, and all samples were reported as % positivity vs corresponding conjugated IgG control; fluorescein isothiocyanate, phycoerythrin and allophycocyanin.

2.4 Metabolic activity

Metabolic activity was measured using resazurin sodium salt (Sigma). A filtered PBS-resazurin solution at 0.01mg/ml with serum-free culture medium was incubated with cells at 37°C for 2H. Resazurin-media was transferred to black 96 well-plates (w/p) (Greiner Bio-One GmbH, Kremsmünster, Austria) and analysed using a FLUOstar Optima plate reader (BMG Labtech, Buckinghamshire, UK) with BMG Lab Tech (Optima, 2.20) software, at excitation 560nm and emission 590nm. Results were analysed using Optima Data Analysis MARS software.

2.5 Co-culture model

24 w/p hanging polyethylene terephthalate (PET) transwell membranes with 1µm pores (Merck, Darmstadt, Germany) were used untreated to seed mono- or co-cultures (Fig. 1A). To mimic the ratio of EC:pericyte coverage in the retina, cells were seeded 1:1 in co-culture. The experimental timescale is outlined in Figure 1B. $2x10^4$ hRP were seeded on the underside of the transwell inserts, in 50µl of complete DMEM with 10% FBS, for 1H at 37°C. Transwells were reverted and placed into a 24 w/p with 900µl of MV medium containing 10% FBS/well. hREC were seeded at $2x10^4$ cells/insert in 200µl MV containing 10% FBS on the apical surface and plates were incubated overnight. For mono-cultures, only 1 cell-type was added (either hRP on the underside or hREC on the apical side). After 24H, inserts were transferred to a new 24 w/p and MV medium was reduced to 5% FBS. 72H after seeding, inserts were cultured in either physiological healthy conditions (20% oxygen + 5.5mM glucose) or 2% oxygen and 33mM glucose, for diabetic-like conditions. Cells were cultured for 21 days with media changed every 3-4 days.

2.6 Human angiogenesis multiplex array

The Q-Plex Human Angiogenesis Array (Quansys, Logan, UT, USA) uses multiplex technology to measure 9 secreted angiogenic proteins of interest: Ang-2, fibroblast growth factor (FGF), hepatocyte growth factor (hHGF), interleukin-8 (IL-8), platelet-derived growth factor-BB (PDGF-BB), tissue inhibitor for metalloproteinase-1 and -2 (TIMP-1/-2), tissue necrosis factor-α (TNFα) and VEGF. 100µl of media was collected from the apical, and 100µl from the outer compartments at 7 time points (Day 0, 3, 7, 10, 14, 17, 21), and stored immediately at -80°C. The assay was performed according to manufacturer's instructions. An 8-point calibration curve was prepared using the calibrator and the human sample diluent, for each plate. Samples were diluted 1:4 and loaded on to the Q-Plex Array 96-w/p. The Q-Plex TM Imager LS and Q-View Imager Pro Software were used for imaging and analysis. Exposure time was 270 seconds. Pericytes from a male donor of unspecified age were used for multiplex run 1, whilst pericytes from a female donor aged 55 were used for runs 2 and 3, as supplied for CellSystems. hREC from the same female donor were used throughout.

2.7 Microscopy

The Nikon DIAPHOT with Top View 3.7 software, and the AxioVert A1 with ZEN Blue 2.3 software were used to capture phase contrast images. The Nikon E-TI, with NIS Elements AR 4.51.01 software was used for cell counts. The Zeiss Confocal M800 with ZEN Blue 2.3 software was used

for imaging cells on glass slides and PET membranes. When imaging co-cultures, PET membranes were removed from their frames and transferred to glass slides.

2.8 Statistical analysis

Statistical analyses were performed using GraphPad Prism 8 software. Significance level of $p<0.05$ was set for all experiments. Data were reported as mean, with standard deviation (SD). ANOVA or non-parametric testing were used for multiple comparisons and T-tests were used for comparisons between two groups.

3. Results

3.1 hREC and hRP maintained their phenotype in vitro within the 21 day experimental timeframe

A limitation of using human primary cells in vitro is their tendency to de-differentiate. hRP maintained their morphology of a large, irregular-shape, with cytoplasmic projections, and did not transition in vitro from P3-P10 (Fig. 2A). hREC retained a cuboidal, uniform size and shape, and formed a monolayer when confluent (Fig. 2B). hRP number increased over time (Fig. 2C), whereas hREC decreased in number from day 7-21 (Fig. 2D). 87.5% of hRP expressed CD146, indicating a heterogeneous population, concomitant with their pluripotent nature (Fig. 2E). hREC were CD34 negative and CD31 positive, which is endothelial specific and present at the border of cell membranes, suggesting hREC retained a strong EC phenotype (Fig. 2F). Both hREC and hRP were CD14 and CD45 negative, distinguishing them from hematopoietic cells. hRP expressed antigens commonly used to confirm pericyte phenotype in culture; PDGFR-β, neuron-glial antigen 2 (NG2) and CD90 (Fig. 2G), and exhibited +/- expression for alpha-smooth muscle actin (α-SMA). hREC expressed a number of key endothelial-specific proteins including vWF, localised to storage vesicles (Weibel-Palade bodies) (Fig. 2H). Positive expression of ZO-1 confirmed TJ formation and VE-Cad confirmed adherens junction formation.

3.2 Both cell-types were viable in sustained hyperglycaemia and hypoxia

Validation of long-term, high glucose and low oxygen conditions was required to induce a diabetic-like phenotype in vitro, whilst aiming to maintain cell viability. hREC and hRP were initially cultured in 5% oxygen to induce a hypoxic response (Fig. S1, Fig. S2). Ang-2 appeared activated in hREC cultured in 5% oxygen (Fig. S1), and SOD-2 appeared activated in hRP cultured in 5% oxygen (Fig. S2). However, oxygen levels were further reduced to 2% after determining only minimal differences compared to 20% oxygen, in both 5.5mM and 33mM glucose conditions. By day 21, the metabolic activity of hRP cultured in 20% oxygen and 30mM glucose was significantly higher than hRP cultured in 5.5mM glucose (Fig. 3A; $p= 0.0434$). There was, however, no significant difference in metabolic activity between hRP cultured in 35mM vs 5.5mM glucose, at day 21 in 20% oxygen ($p>0.999$). Importantly, by day 21 in 20% oxygen, there were fewer hRP in 35mM compared to 5.5mM glucose conditions ($p=0.0002$), suggesting hyperglycaemia at 35mM caused higher metabolic activity/cell in the hRP. By day 21 in hypoxia (2% oxygen), hRP had significantly higher metabolic activity when cultured in 20mM, 25mM and 30mM glucose compared to those cultured in 5.5mM glucose (Fig. 3B; $p=0.0456$, $p=0.0342$, $p=0.0018$, respectively), whilst there was no metabolic difference between hRP cultured in 35mM vs 5.5mM glucose. There was however, significantly more hRP at day 21 in 2% oxygen and 35mM glucose, compared to 2% oxygen and 5.5mM glucose (Fig. 3B; $p<0.0001$), suggesting a lower metabolic activity/cell in the hyperglycaemic-hypoxic conditions. hREC cultured in 20% oxygen with 10-30mM glucose all had significantly lower metabolic activity at day 21 compared to 5.5mM glucose (Fig. 3C; $p=0.0011$

10mM, p=0.0069 15mM, p=0.0048 20mM, p=0.0074 25mM and p=0.0018 30mM). But, there was no significant difference between hREC metabolic activity in 5.5mM vs 35mM in 20% oxygen at day 21. There was however, significantly more hREC at day 21 in 20% oxygen in 5.5mM vs 35mM glucose (Fig. 3C; p=0.0058). Taken together these data suggest hyperglycaemia at 35mM causes higher metabolic activity/cell for hREC cultured in 20% oxygen at day 21 compared to 5.5mM. In 2% oxygen, there was no difference in hREC metabolic activity in 5.5mM- 35mM glucose and also no significant difference in cell number (Fig. 3D). There were no significant differences between 5.5mM glucose and 29.5mM Mannitol + 5.5mM glucose conditions for all experiments by day 21, controlling for the potential confounding osmotic effects of increasing glucose.

3.3 Hypoxic conditions caused re-arrangement of the F-actin cytoskeleton, increased Ang-2 expression and caused hREC hypertrophy

Changes to the hREC monolayer were explored to understand the effect of diabetic-like conditions on microvascular EC behaviour. There was no difference in surface antigens expression when using flow cytometry to compare day 0, day 21 healthy and day 21 diabetic hREC cultured on TC-plastic (Fig. 4A). For hREC mono-cultured on glass slides, ZO-1, VE-Cad and CD31 localised at cell-cell junctions in the four experimental oxygen/glucose conditions at day 21 (Fig. 4B). Cytoskeletal F-actin was arranged in thick stress-fibre-like bands at the borders of the hREC cultured in 2% oxygen, whereas in 20% oxygen the F-actin was dispersed in thin fibres throughout the cell. Connexin-43 (Cx43) was expressed at both the cell-cell junctions and in the perinuclear compartment of mono-cultured hREC. However, in 2% oxygen, Cx43 was predominantly at the cell-cell junctions, indicating an increase in GJ formation. Ang-2 expression in hREC was higher in low oxygen conditions. The cell area of hREC cultured in 2% oxygen +33mM glucose was larger than those cultured in 20% oxygen +5.5mM glucose (Fig. 4C; p=0.0006). There were also more very large cells in 2% oxygen, although the number of focal adhesions per cell was not influenced by oxygen/glucose conditions (Fig. 4D).

3.4 hRP cultures were heterogeneous indicated by αSMA and CD146 expression

Cell surface antigen expression and growth of hRP in response to healthy or diabetic-like conditions were investigated. hRP CD90 expression was retained throughout the 21 day culture period (Fig. 5A), confirming a pericyte phenotype was maintained. CD105 expression was significantly reduced by day 21 in healthy hRP compared to day 0 hRP (p=0.0483). CD146 appeared reduced at day 21 in both healthy and diabetic conditions, however, due to the large variation of CD146 expression in day 0 hRP cultures this was not statistically significant. Irrespective of culture condition, cell density or passage number, only a proportion of hRP expressed αSMA (Fig. 5B). Cytoplasmic protrusions of αSMA-positive hRP were visible through the 1μm pores of the PET in mono-cultures (Fig. 5C), and in co-cultures, where hREC were co-cultured with and without a tight monolayer apically (Fig. 5D and Fig. 5E, respectively), demonstrating physical cell-cell contacts between hREC and hRP.

3.5 Mono- and co-cultured hREC maintained a monolayer in both in healthy and diabetic conditions

Confocal immunofluorescence (IF) analysis of cells on PET membranes at day 21 confirmed hREC and hRP viability, and antibody labelling was used to analyse the EC barrier and assess oxidative and angiogenic responses. The expression of junctional, angiogenic and oxidative stress proteins by hREC cultured on PET for earlier time points of 7 and 14 days is shown in Fig. S3. At day 21, mono-cultured hREC expressed VE-Cad and ZO-1 at cell-cell junctions, in both healthy and diabetic conditions, on PET (Fig. 6A). The Cx43 expression pattern appeared more punctate and dense, in peripheral clusters in the diabetic mono-culture compared to healthy, but overall was less distinct at the cell-cell border on PET, when compared to hREC cultured for 21 days on tissue culture (TC)-treated glass (Fig. 4B). F-actin arrangement was aligned in parallel fibres in healthy mono-cultured hREC, compared to a more disorganised arrangement in diabetic conditions. The distinct 'actin-banding' on the hREC periphery when cultured in 2% oxygen on TC-treated glass (Fig. 4B), was not present when hREC were cultured on PET (Fig. 6A). Some of the differences reported between hREC cultured on TC-treated glass and PET may be due to differences in substrate stiffness and therefore, cell-ECM interaction, or the practicalities of imaging cells on the PET membranes. Z-stack imaging provided confirmation that both cell-types were present on either side of the PET membranes in the co-culture model. ZO-1 and VE-Cad were present at cell-cell borders of co-cultured hREC in both healthy and diabetic conditions, although their expression appeared more uniform in diabetic conditions (Fig. 6B). Cx43 expression was more defined at cell-cell borders in diabetic co-cultured hREC, compared to healthy co-culture. Overall, the EC barrier appeared present in both mono- and co-culture conditions, and unexpectedly was present in diabetic conditions at day 21, subjected to continuous hyperglycaemic and hypoxic insult. HIF1α expression appeared more perinuclear in diabetic co-culture compared to healthy co-cultures at day 21 (Fig. 6B), although overall the HIF1α results were inconclusive when analysed via IF. F-actin arrangement in healthy co-cultured hREC was not aligned in thick parallel fibres like it was in mono-cultured hREC on PET (Fig. 6A) and TC-treated glass (Fig. 4B), suggesting fewer stress fibres within the hREC when co-cultured with pericytes.

3.6 Ang-2, VEGF and PDGF were significantly higher in diabetic conditions

To confirm a diabetic-like phenotype, secretion of the growth factors Ang-2, VEGF and PDGF were assessed for hREC and hRP grown individually and as co-culture, using multiplex analysis. Micrographs of the mono- and co-cultured hREC and hRP confirm the presence of the cells on the PET inserts in healthy and diabetic conditions at days 7, 14 and 21 (Fig. S4). Ang-2 was not secreted by mono-cultured hRP at any time point (Fig. 7A). Ang-2 secreted by diabetic mono-cultured hREC and diabetic co-culture was more than double that of healthy by day 7 (Fig. 7B,C, $p=0.0001$ and $p=0.0002$). From days 7-21, Ang-2 remained significantly higher in diabetic conditions for both mono-cultured hREC and co-cultures. Although Ang-2 was not secreted by hRP, the presence of hRP in co-culture caused a 25.6% increase in secretion of Ang-2 in healthy

co-cultures, and 13.9% increase in diabetic co-cultures (Fig. 7C), compared to mono-cultured hREC at day 21 (Fig. 7B). VEGF was only secreted by hRP (Fig. 7D, E). VEGF was significantly higher in diabetic hRP vs healthy, at day 3 (p=0.0055), 7 (p=0.0093), 14 (p=0.0199) and 21 (p=0.0019) (Fig. 7D). From day 3-17, diabetic VEGF levels were more than double those in healthy conditions, and by day 21, were 3 times higher in diabetic hRP (p=0.0019). VEGF levels in co-culture were very low, suggesting the presence of hREC caused a reduction of VEGF secretion by the hRP (Fig. 7F). Similar to Ang-2, PDGF was secreted at very low/negligible levels by hRP (Fig. 7G). By day 21, PDGF was 2.3-fold higher in diabetic hREC compared to healthy (Fig. 7H; p=0.0008) and 4.4-fold higher in diabetic co-culture vs healthy (Fig. 7I; p=0.0062). PDGF only reached significantly higher levels in diabetic mono-cultured hREC compared to healthy conditions at day 17 onwards (p=0.0158). Although hRP only secreted very low levels of PDGF, in co-culture the levels of PDGF in diabetic conditions exceeded what would be an additive effect of hREC and hRP alone, suggesting in diabetic but not healthy co-culture, higher levels of PDGF were secreted in the presence of hRP. These data support the strength of using long-term co-cultures to explore cellular changes when modelling DR.

3.7 hHGF, TIMP-2 and IL-8 were significantly reduced in diabetic conditions

A panel of proteins including hHGF, TIMP-2 and IL-8 were analysed to determine if the experimental diabetic conditions of the model were sufficient to induce differences to the secretion profile of hREC and hRP, and also assess if there was any paracrine effects when the cells were co-cultured. hHGF was secreted by mono-cultured hRP (Fig.7J), but was not secreted by mono-cultured hREC at any time point (Fig. K). hHGF secretion was significantly lower in diabetic conditions from day 7 in mono-cultured hRP (Fig. 7J; p=0.0146) and co-culture (Fig. 7L; p=0.012), and remained significantly reduced in diabetic co-culture at day 21 (p=0.0303). Levels of hHGF in healthy and diabetic co-culture were lower than secretion levels by mono-cultured hRP at all time points, suggesting the presence of hREC in the co-culture caused a reduction in the overall secretion levels of hHGF. TIMP-2 was secreted by mono-cultured hRP (Fig.7M) and mono-cultured hREC (Fig.7N). TIMP-2 secretion was significantly reduced in diabetic conditions for mono- and co-culture models. This reduction was significant by day 14 in mono-cultured hRP (Fig.7M; p=0.0011), by day 10 in mono-cultured hREC (Fig. 7N; p=0.0451) and day 7 in the co-culture (Fig. 7O; p=0.0165). At day 21, diabetic mono-cultured hREC secreted significantly less TIMP-2 (Fig. 7N; p=0.0026), as did the diabetic co-culture, compared to healthy (Fig. 7O; p=0.0231). Overall TIMP-2 levels were highest in healthy co-culture at day 21, and this appears to be an additive effect of both hREC and hRP secreting TIMP-2. Although hHGF levels remained relatively consistent over time (Fig. 7J-L), IL-8 and TIMP-2 secretion increased in both healthy and diabetic conditions over time (Fig. 7M-R). Both mono-cultured hRP and hREC secreted IL-8 (Fig. 7P,Q) and it appeared that the levels of IL-8 in co-culture may be additive (Fig. 7R). Diabetic conditions caused a significant reduction in IL-8 by mono-cultured hRP at day 14 (Fig. 7P; p=0.0499), and although there was a trend for reduced IL-8 in diabetic mono-cultured hREC and the co-culture, the

reduction was not significant. The large standard deviation across several of the proteins analysed may be in part due to a different hRP donor being used in run 1. Data from all 3 repeats indicate a similar trend, with varying magnitude, for mono-cultured hRP and hREC (Fig. S5), and the co-culture (Fig. S6), in healthy and diabetic-like conditions over time. Overall, the angiogenic protein release profiles highlight that hREC and hRP secreted different proteins, and that one cell-type can have a paracrine effect on the other, as was the case with Ang-2, VEGF, PDGF and hHGF.

4. Discussion

The aim of this study was to develop a human primary, retina-specific, microvascular co-culture model to provide an in vitro environment to study cellular changes, disease progression and future cellular or pharmacological intervention for conditions such as DR. To induce a diabetic-like phenotype in vitro, simultaneous hyperglycaemia and hypoxia culture conditions were used. The key findings of this study were; (1) Human primary hREC and hRP maintained their phenotype and could be cultured together in vitro, (2) high glucose and low oxygen (in vitro diabetic-like) conditions caused an angiogenic response, (3) when hREC and hRP were co-cultured, their angiogenic response was different to mono-cultured cells, and (4) the extended 21 day timescale for experiments was important, as some changes in angiogenic response proteins were only observed at later time points.

An in vitro model should mimic the in vivo situation as closely as possible, while recognising it may have limitations. Co-culturing primary, tissue-specific cells whilst ensuring that they retain their phenotype over time is one option for producing a simplified, reproducible in vitro model to study DR. Human primary vascular ECs from various organs/tissues, including the retina, are commercially available and ECs isolated from different organs are reported to behave differently (Craig et al., 1998). In addition, it has been shown that ECs sourced from larger vessels differ to those from microvasculature (Browning et al., 2012; Solomon et al., 2016). In this study we used human, primary, retinal microvascular cells (hREC) and demonstrated that they retained their cell-specific markers up to 21 days in culture in both healthy and diabetic-like conditions, in contrast to other studies which used animal, immortalised or large vessel co-culture models (Kumar et al., 2011; Tarallo et al., 2012a; Walshe et al., 2011; Wisniewska- Kruk et al., 2012). It is well known that hRP morphology enables them to wrap around the perivascular surface of ECs, sharing physical contact through a shared BM and communicating via paracrine signalling (Pfister et al., 2013). This function has been observed in vitro when ECs and pericytes form structured tubules when cultured together in 3D gels (Stratman et al., 2016; Urich et al., 2013; Zouani et al., 2013). Some of the documented paracrine interactions of hREC and hRP include, PDGF-β, TGF-β and Ang-1/2 signalling, as well as adhesion plaque formation connecting ECs and pericytes, which enables transmission of contractile forces, affecting vessel stability (Tell et al., 2006). In the present study, cells were cultured on either side of transwell inserts and αSMA-positive hRP formed cytoplasmic protrusions through the 1µm pores in the PET membrane, allowing direct physical contact in some areas, which should be taken into account when analysing the data. A major focus of this study was the integrity of the endothelial monolayer, where ZO-1, VE-Cad and Cx43 expression at cell-cell junctions was used to confirm barrier homeostasis and effective cell-cell communication. hREC formed a monolayer, with ZO-1 and VE-cad present at cell-cell borders in both mono- and co-cultures. Contrary to reports by other groups, hRP and hREC can be maintained in vitro (Berrone et al., 2009; Kashyap et al., 2013;), and cultured together, with no

clear indication of phenotypic switch, due to carefully adjusted culture conditions, rendering this model an improvement upon immortalised, animal, or large vessel co-culture options.

Establishing the appropriate conditions of a disease model can be challenging, in particular, when modelling a chronic disease with multiple confounding co-morbidities. Throughout onset and progression of diabetes, capillary ECs and the perivascular pericytes progressively deteriorate due to hyperglycaemia. Disturbance to the capillary ECs, caused by EC and/or pericyte drop-out or capillary bed regression, can result in disrupted blood flow and eventually vessel occlusion, which in turn leads to ischemia, hypoxia and non-perfusion to the underlying retinal tissue. Our model aimed to represent vessels that have been subjected to high glucose insult due to diabetes, and also reduced oxygen, due to loss of BRB integrity and regression of the retinal capillary bed. The in vitro conditions were carefully developed to attempt to maintain a healthy phenotype, or induce a diabetic-like phenotype for the hREC and hRP, within a comparatively short timeframe relative to the progressive onset of diabetes in a patient. 1-2% oxygen has been used previously in studies investigating the effect of hypoxia on cells in vitro (Kumar et al., 2011; Liu et al., 2006; Oh et al., 1999), therefore we chose 2% oxygen to maintain viability of the cells in the relatively long term culture period of the mono- and co-culture model in this study. Several groups have used 20-35mM [D]+ glucose to model diabetes in vitro, with 25mM being the most common (Amano et al., 2005; Giebel et al., 2005; Ho et al., 2000; Nyengaard et al., 2004; Piconi et al., 2004; Risso et al., 2001; Romeo et al., 2002; Trudeau et al., 2011). In a more recent tri-culture, human, retina-specific study, 40mM glucose was used to assess short term cellular response to hyperglycaemia (Fresta et al., 2020). We determined that glucose levels between 30-35mM had a metabolic effect on both hRP and hREC in vitro, which led to 33mM being used to model hyperglycaemia in this study, as others have done (Ho, et al., 2000).

Hypoxia-induced oxidative stress plays a crucial role in DR progression (Li et al, 2012), and combined hyperglycaemia and low oxygen was expected to lead to hRP cell loss in vitro. But surprisingly, hRP thrived in low oxygen, high glucose conditions. However, in vitro hRP are more prone to apoptosis in fluctuating high glucose compared to sustained high glucose, which was used in the present study (Busik et al., 2008; Tarallo et al., 2012b). Oxygen levels in the retina have been reported to range from 1-5% (Ivanovic, 2009). Therefore, it may be due to fact that the hREC and hRP used in this study are primary cells and so are more robust against hypoxic insult than the immortalised or large vessel EC/pericytes that have previously been used in similar models. The unexpected trend of increased cell junction localisation of Cx43, ZO-1 and VE-Cad suggests the hREC monolayer barrier integrity was in fact enhanced by the low oxygen, high glucose environment, contrary to reports of disrupted EC integrity in the progression of diabetes (Singh et al., 2014). Various groups have suggested Cx43 expression is affected by diabetic culture conditions (Kuo et al., 2020; Roy et al., 2017). In the present study, Cx43 clustered specifically at hREC cell-cell junctions in low oxygen, compared to dispersed throughout the

cytoplasm with less specificity to the cell-cell junctions in healthy conditions. This indicates GJ activity was highly dynamic and was affected by oxidative and hyperglycaemic stress. It is possible that cells in sustained diabetic conditions have undergone an adaptive remodelling response, which may not have occurred if parameters such as fluctuating glucose, manipulation of the ECM, the addition of flow and of other perivascular cells, such as astrocytes, were included. However, those additions were beyond the scope of this particular study.

Angiogenic signalling pathways are also heavily implicated in pericyte:EC homeostasis. Ang-2, VEGF, and PDGF secretion were all higher, whilst hHGF, TIMP-2 and IL-8 secretion were all reduced in diabetic-like compared to healthy conditions in this study. Alteration to the levels of these proteins will disrupt multiple signalling pathways involved in homeostasis, wound healing and vascular health. Intravitreal injection of anti-VEGF agents is the current gold standard for treating late stage DR, once PDR begins to cause vision problems (Medina et al., 2013). VEGF levels increase in the ocular fluid of patients with varying stages of DR, particularly during PDR (Baharivand et al., 2012). VEGF is a driver of pathological angiogenesis in ischemic and inflammatory diseases (Witmer et al., 2003)**,** and in this study, was significantly higher in pericytes cultured in diabetic-like conditions, compared to healthy. Interestingly, very low/out of range levels of VEGF were detected in co-culture conditions, highlighting that the presence of hREC altered the secretion behaviour of hRP.

A second major angiogenic driver is Ang-2, where Ang-2 outcompetes Ang-1 for Tie-2 receptor binding, resulting in destabilisation of the vasculature (Thurston et al., 2013). Ang-2 was upregulated in hREC mono-cultured in low oxygen for 21 days and secretion was significantly higher from day 7 in diabetic mono- and co-cultures compared to healthy conditions. High Ang-2 levels have previously been reported in hREC cultured in diabetic conditions (Rangasamy et al., 2011), and novel treatments for DR based on targeting Ang-2 are currently in early stage clinical trials (Stewart, 2017; Tell et al., 2006). It has been documented that brain microvascular ECs and rat brain pericytes have differential responses to glucose deprivation and hypoxia, with ECs displaying F-actin rearrangement within 24H exposure (Engelhardt et al., 2015), and similarly, in the present study there was F-actin rearrangement in hypoxic hREC, from dispersed, thin filaments in healthy conditions to increased numbers of thick peripheral stress fibres, a feature of many different types of hypoxic ECs in culture (Zieseniss, 2014). Human brain microvascular ECs cultured under hypoxia plus inflammatory activation using IL-1β, displayed F-actin rearrangement from a small number of thin, dispersed filaments in healthy conditions, to numerous, parallel thick fibres (Tang et al., 2020), similar to the stress-like fibres formed by hREC in the present study when cultured under hypoxic/high glucose conditions. This confirms the high glucose and low oxygen conditions activated signalling pathways involved in re-arrangement of the hREC cytoskeleton. We speculate that the difference in cell culture surface characteristics will effect cell-ECM adhesion, which may also have affected F-actin alignment in hREC, accounting for the

differences observed between cells cultured on glass or PET. The presence of pericyte protrusions through the PET in co-culture may also affect hREC adhesion, resulting in F-actin re-arrangement. Interestingly, hREC also had a larger surface area by day 21 in hypoxic conditions, and this cell hypertrophy may be a cellular response to hypoxia; to increase oxygen diffusion across a larger surface area. Combined, increased VEGF and Ang-2, dynamic GJ activity, and actin cytoskeleton rearrangement indicate that the in vitro diabetic conditions initiated an angiogenic response.

Traditional cell culture does not take into consideration the paracrine or structural effect of neighbouring cell-types. Therefore, to understand changes in the retinal microvasculature, where pericyte coverage is very high, developing a co-culture of 1:1 hRP and hREC, with shared basement membrane (BM) mimic, has provided valuable data on the cellular changes in diabetes. Others have highlighted the influencing effect of growth factors released from neighbouring cells on EC behaviour (Dohgu et al., 2005; Gardner et al., 1997), hence underlining the benefit of using co-culture models as opposed to traditional mono-cultures. Our results confirmed that the angiogenic secretion profile and EC barrier integrity differed between mono- and co-cultures. Re-arrangement of the F-actin cytoskeleton in the co-culture vs hREC mono-culture and the observation of reduced junction-specific ZO-1, VE-Cad and Cx43 in co-culture supports the hypothesis that long-term co-culture affects hREC structure and monolayer integrity.

Assessing the secretion profile of mono-cultured and co-cultured cells in either healthy or diabetic conditions enabled assessment of cellular changes due to diabetic-like insult, as well as paracrine effects of neighbouring cells simultaneously. TIMP-2 is important for maintaining ECM homeostasis, and in pathological conditions such as DR the TIMP:matrix metalloproteinase (MMP) ratio can affect capillary BM thickening at an early stage (Castruita-De la Rosa et al., 2017; Roy et al., 2010). Reduced TIMP-2 levels may result in increased MMP activity, leading to increased ECM remodelling, and disruption to normal cell function, adhesion, and cell:cell communication, mimicking an angiogenic switch. TIMP-2 was secreted by both hRP and hREC, and was reduced in diabetic conditions in mono- and co-cultures. Ang-2 levels in co-culture were overall higher than hREC mono-culture, in both healthy and diabetic conditions, suggesting hREC secreted more Ang-2 in the presence of hRP. hRP in mono-culture did not secrete Ang-2 at all. In a mouse study, high glucose caused Ang-2 induced pericyte apoptosis via α3β1 integrin (Park et al., 2014), suggesting raised Ang-2 may be responsible for the early-drop out of pericytes, a common observation in diabetic retinae (Motiejunaite and Kazlauskas, 2008)**.** Many studies using both animal and human retinae found Ang-2/Tie signalling was critical for pericyte survival and interaction with underlying EC, wherein increased Ang-2 leads to unstable pericyte:EC contact points (Bergers and Song, 2005; Hammes et al., 2004). Considering hRP did not secrete Ang-2 at all, the co-culture model is vital to highlight the differential secretion profiles of hREC and hRP, the effect each has on one another and to truly understand changes occurring in the retinal microvasculature.

Similarly, hREC did not secrete hHGF and hRP did not secrete PDGF, although their presence appeared to alter the secretion profile when in co-culture. hHGF, or scatter factor, has been described as both an adipocytokine and a hepatokine (Balaban et al., 2006), which has a role in metabolic flux of glucose in various insulin-sensitive cells, with growing evidence suggesting hHGF plays a role in metabolic disorders such as type 2 diabetes (Oliveira et al., 2018). A comprehensive study comparing human patients at various stages of eye disease, found vitreous hHGF levels significantly increase depending on severity of retinopathy (Nishimura et al., 1999). In the present study, however, hHGF was lower in diabetic-like conditions at all time points. Also, hHGF was reduced in both healthy and diabetic co-cultures compared to mono-culture hRP, suggesting the presence of hREC reduced the overall hHGF secretion. This paracrine effect is of vital importance when aiming to model a disease where ECs and pericytes appear to significantly influence one-another's secretion profile. PDGF is an important growth factor for all phases of wound healing as well as a potent mitogen for mesenchymal cells (Goksen et al., 2017). In a study focused on diabetic nephropathy, urinary excretion rates of PDGF-BB were significantly increased congruent to urine albumin excretion (Wang et al., 2009). This implies PDGF-BB may play a role in the onset of diabetes, linked with early microvascular changes. In the present study, hRP secreted very low/ undetectable PDGF within the 21 day timeframe. However, secretion of PDGF was higher in diabetic co-culture compared to mono-cultured hREC, suggesting the presence of a second cell-type (hRP) in the co-culture changes the secretion profile. These results imply hREC and hRP have paracrine effect on the angiogenic secretion profile of one another, within the experimental parameters. This emphasises the value of a simplified in vitro co-culture model for unravelling the fundamental cellular changes in DR and for testing novel therapeutic targets in the future.

When attempting to fully understand the stages of cellular alterations in a progressive disease, the value of collecting data over multiple time points is irrefutable. Data analysis at 7 time points, over 21 days, has provided insight into cell behaviour over time, compared to previously published co-culture models which range in time scale from: 24h, 2, 3 and 8 days (Hayashi et al., 2004; Tarallo et al., 2012a; Wisniewska-Kruk et al., 2012). Ang-2, PDGF, TIMP-2 and IL-8 secretion all increased over time. In particular, PDGF was significantly higher in diabetic mono-cultured hREC and co-culture, but only from day 17 and 21 respectively. In contrast, VEGF data suggests a diabetic-like state was induced in hRP in a relatively short culture time. Collection of data at multiple time points, over a long-term culture period helps to understand the chronology of changing cell behaviour related to the progression of DR.

5. Conclusions

These data confirm successful long term culture of stringently characterised hREC and hRP, individually and in co-culture. Introducing carefully selected in vitro healthy and diabetic-like conditions enabled data collection at multiple time points over 21 days and differences in the

angiogenic secretion profile of healthy compared to diabetic cells suggested an angiogenic switch in the low oxygen, high glucose environment. Significant differences were also discovered in mono- vs co-cultures, highlighting the importance of studying the behaviour of hRP and hREC together, rather than in isolation. This in vitro co-culture model could help unravel cell signalling changes caused by diabetes, and offer a reproducible model to assess novel pharmaceutical interventions aimed at targeting early stage DR.

Acknowledgements

Thanks to Oxford Biosystems Ltd for their technical support with the angiogenesis multiplex arrays.

Data Availability

The datasets generated during and/or analysed during the current study are available from the corresponding author on reasonable request. Before publication, files will be made accessible via online repository.

Contribution statement

Data was collected by Jessica J Eyre. Jessica J Eyre, Rachel L Williams and Hannah J Levis all contributed to conception and experimental design, interpretation of data, drafting of the article and final approval of the published version. Hannah J Levis is the guarantor.

References

Amano, S., Yamagishi, S.I., Inagaki, Y., Nakamura, K., Takeuchi, M., Inoue, H., Imaizumi, T., 2005. Pigment epithelium-derived factor inhibits oxidative stress-induced apoptosis and dysfunction of cultured retinal pericytes. Microvasc. Res. 69, 45–55. https://doi.org/10.1016/j.mvr.2004.11.001

Antonetti, D.A., Barber, A.J., Bronson, S.K., Freeman, W.M., Thomas, W., Jefferson, L.S., Kester, M., Kimball, S.R., Krady, J.K., Kathryn, F., Norbury, C.C., Quinn, P.G., Sandirasegarane, L., Simpson, I.A., 2004. Perspectives in Diabetes Diabetic Retinopathy: Seeing Beyond Glucose-Induced Microvascular Disease. Diabetes. 55, 2401–2411. https://doi.org/10.2337/db05-1635

Balaban, Y.H., Sumer, H., Simsek, H., Us, D., Tatar, G., 2006. Metabolic syndrome, non-alcoholic steatohepatitis (NASH), and hepatocyte growth factor (HGF). Ann. Hepatol. 5, 109–114. https://doi.org/10.1016/S1665-2681(19)32027-7

Baharivand, N., Zarghami, N., Panahi, F., Ghafari, M.Y.D., Fard, A.M., Mohajeri, A., 2012. Relationship between vitreous and serum vascular endothelial growth factor levels, control of diabetes and microalbuminuria in proliferative diabetic retinopathy. Clin. Ophthalmol. 6, 185–191. https://doi.org/10.2147/OPTH.S27423

Bergers, G., Song, S., 2005. The role of pericytes in blood-vessel formation and maintenance. Neuro. Oncol. 7, 452–464. https://doi.org/10.1215/S1152851705000232

Berrone, E., Beltramo, E., Buttiglieri, S., Tarallo, S., Rosso, A., Hammes, H., Porta, M., 2009. Establishment and characterization of a human retinal pericyte line : A novel tool for the study of diabetic retinopathy. Int J Mol Med. 23, 373–378. https://doi.org/10.3892/ijmm

Browning, A.C., Halligan, E.P., Stewart, E.A., Swan, D.C., Dove, R., Samaranayake, G.J., Amoaku, W.M., 2012. Comparative gene expression profiling of human umbilical vein endothelial cells and ocular vascular endothelial cells. Br. J. Ophthalmol. 96, 128–132. https://doi.org/10.1136/bjophthalmol-2011-300572

Busik, J. V., Mohr, S., Grant, M.B., 2008. Hyperglycemia-Induced reactive oxygen species toxicity to endothelial cells is dependent on paracrine mediators. Diabetes 57, 1952–1965. https://doi.org/10.2337/db07-1520

Castruita-De la Rosa, C., Garza-Veloz, I., Cardenas-Vargas, E., Castañeda-Miranda, R., Solis-Sanchez, L.O., Ortiz-Rodriguez, J.M., Vega-Carrillo, H.R., Martinez-Blanco, M.R. Flores-Morales, V., Hernandez-Delgadillo, G.P., Badillo-Almaráz, J.I., Martinez-Fierro, M.L., 2017. Biological Activity and Implications of the Metalloproteinases in Diabetic Foot Ulcers. Intech open 169–190. http://dx.doi.org/10.5772/intechopen.71725

Craig, L.E., Spelman, J.P., Strandberg, J.D., Zink, M.C., 1998. Endothelial Cells from Diverse Tissues Exhibit Differences in Growth and Morphology. Microvasc. Res. 76, 65–76. https://doi.org/10.1006/mvre.1997.2045

Dohgu, S., Takata, F., Yamauchi, A., Nakagawa, S., Egawa, T., Naito, M., Tsuruo, T., Sawada, Y., Niwa, M., Kataoka, Y., 2005. Brain pericytes contribute to the induction and up-regulation of blood-brain barrier functions through transforming growth factor-β production. Brain Res. 1038, 208–215. https://doi.org/10.1016/j.brainres.2005.01.027

Engelhardt, S., Huang, S., Patkar, S., Gassmann, M., Ogunshola, O.O., 2015. Differential responses of blood-brain barrier associated cells to hypoxia and ischemia: a comparative study. Fluids Barriers CNS. 12, 1-16. http://doi.org/10.1186/2045-8118-12-4

Fresta, C.G., Fidilio, A., Caruso, G., Caraci, F., Giblin, F.J., Leggio, G.M., Salomone, S., Drago, F., Bucolo, C., 2020. A New Human Blood – Retinal Barrier Model Based on Endothelial Cells, Pericytes, and Astrocytes Int. J. Mol. Sci. 21, 1–17. https://doi.org/10.3390/ijms21051636

Gardner, T.W., Lieth, E., Khin, S.A., Barber, A.J., Bonsall, D.J., Lesher, T., Rice, K., Brennan, W.A., 1997. Astrocytes increase barrier properties and ZO-1 expression in retinal vascular endothelial cells. Investig. Ophthalmol. Vis. Sci. 38, 2423–2427.

Giebel, S.J., Menicucci, G., McGuire, P.G., Das, A., 2005. Matrix metalloproteinases in early diabetic retinopathy and their role in alternation of the blood-retinal barrier. Lab. Investig. 85, 597–607. https://doi.org/10.1038/labinvest.3700251

Goksen, S., Balabanli, B., Coskun-Cevher, S., 2017. Application of platelet derived growth factor-BB and diabetic wound healing: the relationship with oxidative events. Free Radic. Res. 51, 498–505. https://doi.org/10.1080/10715762.2017.1327715

Hammes, H.P., Lin, J., Wagner, P., Feng, Y., Vom Hagen, F., Krzizok, T., Renner, O., Breier, G., Brownlee, M., Deutsch, U., 2004. Angiopoietin-2 Causes Pericyte Dropout in the Normal Retina: Evidence for Involvement in Diabetic Retinopathy. Diabetes. 53, 1104–1110. https://doi.org/10.2337/diabetes.53.4.1104

Hayashi, K., Nakao, S., Nakaoke, R., Nakagawa, S., 2004. Effects of hypoxia on endothelial / pericytic co-culture model of the blood – brain barrier. Regul Pept. 123, 77–83. https://doi.org/10.1016/j.regpep.2004.05.023

Ho, F.M., Liu, S.H., Liau, C.S., Huang, P.J., Lin-Shiau, S.Y., 2000. High glucose-induced apoptosis in human endothelial cells is mediated by sequential activations of c-JUN NH2-terminal kinase and caspase-3. Circulation. 101, 2618–2624. https://doi.org/10.1161/01.CIR.101.22.2618

Ivanovic, Z., 2009. Hypoxia or in situ normoxia: The stem cell paradigm. J. Cell. Physiol. 219, 271–275. https://doi.org/10.1002/jcp.21690

Kashyap, M. V, Ranjan, A.P., Shankardas, J., Vishwanatha, J.K., 2013. Establishment of Human Retinal Microvascular Endothelial Cells with Extended Life-span. In Vivo. 27, 685–694.

Kowluru, R.A., Zhong, Q., Kanwar, M., 2010. Metabolic memory and diabetic retinopathy: Role of inflammatory mediators in retinal pericytes. Exp. Eye Res. 90, 617–623. https://doi.org/10.1016/j.exer.2010.02.006

Kumar, R., Harris-hooker, S., Kumar, Ritesh, Sanford, G., 2011. Co-culture of Retinal and Endothelial Cells Results in the Modulation of Genes Critical to Retinal Neovascularization. Vasc. Cell. 3, 1-15. https://doi.org/10.1186/2045-824X-3-27

Kuo, C., Green, C.R., Rupenthal, I.D., Mugisho, O.O., 2020. Connexin43 hemichannel block protects against retinal pigment epithelial cell barrier breakdown. Acta Diabetol. 57, 13–22. https://doi.org/10.1007/s00592-019-01352-3

Li, S.-Y., Fu, Z.J., Lo, A.C.Y., 2012. Hypoxia-Induced Oxidative Stress in Ischemic Retinopathy. Oxid. Med. Cell. Longev. 2012, 1–10. https://doi.org/10.1155/2012/426769

Liu, L., Cash, T.P., Jones, R.G., Keith, B., Thompson, C.B., Simon, M.C., 2006. Hypoxia-induced energy stress regulates mRNA translation and cell growth. Mol. Cell. 21, 521–531. https://doi.org/10.1016/j.molcel.2006.01.010

627 Medina, R.J., O'neill, C.L., O'doherty, T.M., Chambers, S.E.J., Guduric-Fuchs, J., Neisen, J.,
628 Waugh, D.J., Simpson, D.A., Stitt, A.W., 2013. Ex vivo expansion of human outgrowth endothelial
629 cells leads to IL-8-mediated replicative senescence and impaired vasoreparative function. Stem
630 Cells. 31, 1657–1668. https://doi.org/10.1002/stem.1414

631 Motiejunaite, R., Kazlauskas, A., 2008. Pericytes and ocular diseases. Exp. Eye Res. 86, 171–177.
632 https://doi.org/10.1016/j.exer.2007.10.013

633 Nishimura, M., Ikeda, T., Ushiyama, M., Nanbu, A., Kinoshita, S., Yoshimura, M., 1999. Increased
634 vitreous concentrations of human hepatocyte growth factor in proliferative diabetic retinopathy. J.
635 Clin. Endocrinol. Metab. 84, 659–662. https://doi.org/10.1210/jc.84.2.659

636 Nyengaard, J.R., Ido, Y., Kilo, C., Williamson, J.R., 2004. Interactions Between Hyperglycemia and
637 Hypoxia Implications for Diabetic Retinopathy. Diabetes. 53, 2931–2938.
638 https://doi.org/10.2337/diabetes.53.11.2931

639 Oh, H., Takagi, H., Suzuma, K., Otani, A., Matsumura, M., Honda, Y., 1999. Hypoxia and vascular
640 endothelial growth factor selectively up-regulate angiopoietin-2 in bovine microvascular endothelial
641 cells. J. Biol. Chem. 274, 15732–9. https://doi.org/10.1074/JBC.274.22.15732

642 Oliveira, A.G., Araújo, T.G., Carvalho, B. M., Rocha, G.Z., Santos, A., Saad, M.J.A., 2018. The
643 Role of Hepatocyte Growth Factor (HGF) in Insulin Resistance and Diabetes. Front. Endocrinol.
644 9,503, 1-10. https://doi.org/10.3389/fendo.2018.00503

645 Park, S.W., Yun, J., Kim, Jin Hyoung, Kim, K., Cho, C., Kim, J.H., 2014. Angiopoietin 2 Induces
646 Pericyte Apoptosis via a α3β1 Integrin Signaling in Diabetic Retinopathy. Diabetes. 63, 3057–3068.
647 https://doi.org/10.2337/db13-1942

648 Pfister, F., Przybyt, E., Harmsen, M.C., 2013. Pericytes in the eye. Eur J Physiol. 465, 789–796.
649 https://doi.org/10.1007/s00424-013-1272-6

650 Piconi, L., Quagliaro, L., Assaloni, R., Giugliano, D., Szabo, C., 2004. Intermittent high glucose
651 enhances ICAM-1, VCAM-1, E-selectin and interleukin-6 expression in human umbilical endothelial
652 cells in culture: the role of poly (ADP-ribose) polymerase. J Thromb Haemost. 12, 1453–1459.
653 https://doi.org/10.1111/j.1538-7836.2004.00835.x

654 Rangasamy, S., Srinivasan, R., Maestas, J., McGuire, P.G., Das, A., 2011. A potential role for
655 angiopoietin 2 in the regulation of the blood-retinal barrier in diabetic retinopathy. Investig.
656 Ophthalmol. Vis. Sci. 52, 3784–3791. https://doi.org/10.1167/iovs.10-6386

657 Risso, A., Mercuri, F., Quagliaro, L., Damante, G., Ceriello, A., 2001. Intermittent high glucose
658 enhances apoptosis in human umbilical vein endothelial cells in culture. Am. J. Physiol. Metab.
659 281, E924–E930. https://doi.org/10.1152/ajpendo.2001.281.5.E924

660 Romeo, G., Liu, W., Asnaghi, V., Kern, T.S., Lorenzi, M., 2002. Activation of Nuclear Factor- κβ
661 Induced by Diabetes and High Glucose Regulates a Proapoptotic Program in Retinal Pericytes.
662 Diabetes. 51, 2241-2248. https://doi.org/10.1155/2012/426769

663 Roy, S., Ha, J., Trudeau, K., Beglova, E., 2010. Vascular basement membrane thickening in
664 diabetic retinopathy. Curr. Eye Res. 35, 1045–1056.
665 https://doi.org/10.3109/02713683.2010.514659

666 Roy, S., Kim, D., Lim, R., 2017. Cell-cell communication in diabetic retinopathy. Vision Res. 139,
667 115–122. https://doi.org/10.1016/j.visres.2017.04.014

668 Singh, V.P., Bali, A., Singh, N., Jaggi, A.S., 2014. Advanced glycation end products and diabetic
669 complications. Korean J. Physiol. Pharmacol. 18, 1–14. https://doi.org/10.4196/kjpp.2014.18.1.1

670 Solomon, I., O-Reilly, M., Ionescu, L. Alphonse, R.S., Rajabali, S., Zhong, S., Vadivel, A., Shelley,
671 W.C., Yoder, M.C., Thébaud, B., 2016. Functional Differences Between Placental Micro- and
672 Macrovascular Endothelial Colony-Forming Cells. Transl Med. 5, 291–300.
673 http://doi.org/10.5966/sctm.2014-0162

674 Stewart, M.W., 2017. Future Treatments of Diabetic Retinopathy : Pharmacotherapeutic Products
675 Under Development. EMJ Diabet. 2017, 93–103.

676 Stitt, A.W., Curtis, T.M., Chen, M., Medina, R.J., McKay, G.J., Jenkins, A., Gardiner, T.A., Lyons,
677 T.J., Hammes, H.P., Simó, R., Lois, N., 2016. The progress in understanding and treatment of
678 diabetic retinopathy. Prog. Retin. Eye Res. 51, 156–186.
679 https://doi.org/10.1016/j.preteyeres.2015.08.001

680 Stratman, A.N., Malotte, K.M., Mahan, R.D., Davis, M.J., Davis, G.E., 2016. Pericyte recruitment
681 during vasculogenic tube assembly stimulates endothelial basement membrane matrix formation.
682 Blood. 114, 5091–5102. https://doi.org/10.1182/blood-2009-05-222364.

683 Tarallo, S., Beltramo, E., Berrone, E., Porta, M., 2012(a). Human pericyte-endothelial cell
684 interactions in co-culture models mimicking the diabetic retinal microvascular environment. Acta
685 Diabetol. 49, S141-S151 https://doi.org/10.1007/s00592-012-0390-5

686 Tarallo, S., Beltramo, E., Berrone, E., Porta, M., 2012(b). Thiamine and beβotiamine prevent
687 apoptosis induced by high glucose-conditioned extracellular matrix in human retinal pericytes.
688 Diabetes Metab Res Rev. 25, 647-656. https://doi.org/10.1002/dmrr.1008

689 Tang, J., Kang, Y., Huang, L., Wu, L., Peng, Y., 2020. TIMP1 preserves the blood–brain barrier
690 through interacting with CD63/integrin β1 complex and regulating downstream FAK/RhoA
691 signaling. Acta Pharm. Sin. B 10, 987–1003. https://doi.org/10.1016/j.apsb.2020.02.015

692 Tell, D. Von, Armulik, A., Betsholtz, C., 2006. Pericytes and vascular stability. Exp Cell Res. 312,
693 623–629. https://doi.org/10.1016/j.yexcr.2005.10.019

694 Thurston, G., Daly, C., Whitehead, K.J., Smith, M.C.P., Li, Y., Lampugnani, M.G., Landskroner-
695 eiger, S., Moneke, I., 2013. The Complex Role of Angiopoietin-2 in the Angiopoietin – Tie Signaling
696 Pathway. Cold Spring Harb Perspect Med. 2, 1–14. https://doi.org/10.1101/cshperspect.a006650

697 Trudeau, K., Molina, A.J.A., Roy, S., 2011. High Glucose Induces Mitochondrial Morphology and
698 Metabolic Changes in Retinal Pericytes. Invest. Ophthalmol. Vis. Sci. 52, 8657–8664.
699 https://doi.org/10.1167/iovs.11-7934

700 Urich, E., Patsch, C., Aigner, S., Graf, M., Iacone, R., Freskgård, P.O., 2013. Multicellular self-
701 assembled spheroidal model of the blood brain barrier. Sci. Rep. 3, 1-8.
702 https://doi.org/10.1038/srep01500

703 Walshe, T.E., Connell, P., Cryan, L., Ferguson, G., Gardiner, T., Morrow, D., Redmond, E.M.,
704 O'Brien, C., Cahill, P.A., 2011. Microvascular retinal endothelial and pericyte cell apoptosis in vitro:
705 Role of hedgehog and notch signalling. Investig. Ophthalmol. Vis. Sci. 52, 4472–4483.
706 https://doi.org/10.1167/iovs.10-7061

707 Wang, Q.Y., Guan, Q.H. & Chen, F.Q., 2009. The changes of platelet-derived growth factor-BB
708 (PDGF-BB) in T2DM and its clinical significance for early diagnosis of diabetic nephropathy.
709 Diabetes Res. Clin. Pract. 85, 166–170. https://doi.org/10.1016/j.diabres.2009.05.008

Wild, S., Roglic, G., Green, A., Sicree, R., King, H., 2004. Estimates for the year 2000 and projections for 2030. Diabetes Care. 27, 1047-1053. http://doi.org/10.2337/diacare.27.5.1047

Wisniewska-Kruk, J., Hoeben, K.A., Vogels, I.M.C., Gaillard, P.J., Van Noorden, C.J.F., Schlingemann, R.O., Klaassen, I., 2012. A novel co-culture model of the blood-retinal barrier based on primary retinal endothelial cells, pericytes and astrocytes. Exp. Eye Res. 96, 181–190. https://doi.org/10.1016/j.exer.2011.12.003

Witmer, a. N., Vrensen, G.F.J.M., Van Noorden, C.J.F., Schlingemann, R.O., 2003. Vascular endothelial growth factors and angiogenesis in eye disease. Prog. Retin. Eye Res. 22, 1–29. https://doi.org/10.1016/S1350-9462(02)00043-5

Yao, D., Taguchi, T., Matsumura, T., Pestell, R., Edelstein, D., Giardino, I., Suske, G., Rabbani, N., Thornalley, P.J., Sarthy, V.P., Hammes, H.P., Brownlee, M., 2007. High glucose increases angiopoietin-2 transcription in microvascular endothelial cells through methylglyoxal modification of mSin3A. J. Biol. Chem. 282, 31038–31045. https://doi.org/10.1074/jbc.M704703200

Yau, J.W.Y., Rogers, S.L., Kawasaki, R., Lamoureux, E.L., Kowalski, J.W., Bek, T., Chen, S.J., Dekker, J.M., Fletcher, A., Grauslund, J., Haffner, S., Hamman, R.F., Ikram, M.K., Kayama, T., Klein, B.E.K., Klein, R., Krishnaiah, S., Mayurasakorn, K., O'Hare, J.P., Orchard, T.J., Porta, M., Rema, M., Roy, M.S., Sharma, T., Shaw, J., Taylor, H., Tielsch, J.M., Varma, R., Wang, J.J., Wang, N., West, S., Zu, L., Yasuda, M., Zhang, X., Mitchell, P., Wong, T.Y., 2012. Global prevalence and major risk factors of diabetic retinopathy. Diabetes Care. 35, 556–564. https://doi.org/10.2337/dc11-1909

Zieseniss, A., 2014. Hypoxia and the modulation of the actin cytoskeleton; emerging interrelations. Hypoxia. 2, 11-21. https://doi.org/10.2147/hp.s53575

Zouani, O.F., Lei, Y., Durrieu, M., 2013. Pericytes, Stem-Cell-Like Cells, but not Mesenchymal Stem Cells are Recruited to Support Microvascular Tube Stabilization. Small. 9, 1–6. https://doi.org/10.1002/smll.201300124

Tables

Table 1: Primary antibodies for immunofluorescence

Antibody	Supplier	Working concentration
anti-αSMA	Abcam, Cambridge, UK, ab7817	5µg/ml
anti-Thy-1/CD90	Abcam, ab23894	2µg/ml
anti-HIF1α	Abcam, ab199004	1µg/ml
anti-VEGFR-2	Abcam, ab9530	5µg/ml
anti-Ang-2	Abcam, ab153934	7.2µg/ml
anti-Desmin	Abcam, ab15200	1.45µg/ml
anti-vWF	Abcam, ab6994	21.5µg/ml
anti-VE-Cad	Abcam, ab33168	3.5µg/ml
anti-CD31	Abcam, ab2836	0.6µg/ml
anti-Cx43	Abcam, ab11370	3.5µg/ml
anti-Paxillin	Abcam, ab32084	1:200
anti-PDGFR-β	Santa Cruz Biotech, Dallas, TX, USA, sc-374573	0.8µg/ml
anti-ZO-1	Invitrogen, Waltham, MA, USA, 61-7300	2.5µg/ml
anti-SOD-2	Fisher Scientific, Loughborough, UK, A21990	5µg/ml
anti-SOD-1	Merck, MABC684	1:200
anti-NG2	Merck, ab5320	5µg/ml

Table 2: Primary antibodies for flow cytometry

Conjugated antibody	Supplier	Volume/test
anti-IgG-1 kappa-FITC	Fisher Scientific, 15104218	5µl/test
anti-IgG-1 kappa-PE	Fisher Scientific, 12611959	5µl/test
anti-IgG-1 kappa-APC	Fisher Scientific, 12642059	5µl/test
anti-CD31-APC	Fisher Scientific, 15577906	5µl/test
anti-CD146-PE	Fisher Scientific, 15546896	5µl/test
anti-CD105-PE	Fisher Scientific, 15576846	5µl/test
anti-CD90-APC	Fisher Scientific, 17090942	5µl/test
anti-CD14-APC	Fisher Scientific, 15517886	5µl/test
anti-CD45-FITC	Fisher Scientific, 15556406	5µl/test
anti-CD34-FITC	Fisher Scientific, 12372223	6µl/test

Figure Legends

Figure 1. Schematic of the *in vitro* setup, seeding method and timescales for the mono/co-culture models

Three models were analysed (**A**): $2x10^4$ hREC only on the apical side of the PET, $2x10^4$ hRP only on the underside of the PET, and the co-culture where $2x10^4$ hREC were seeded on the apical side and $2x10^4$ hRP seeded on the underside of the PET transwell insert at a 1:1 ratio. The method for seeding the cells is illustrated in **B**. Cells were seeded onto inserts as shown and placed in a 24 w/p. Incubation steps were at 5% CO_2 in air and 37°. For hREC only and hRP mono-cultures, only one cell-type was added to the insert. Cells were cultured for 21 days. Media samples were collected at day 0, 3, 7, 10, 14, 17 and 21 for multiplex analysis. This figure was created with BioRender.com.

Figure 2. Characterisation of hRP and hREC

A and **B**: Light micrographs illustrating the morphology of hRP and hREC cultured individually on TC plastic at passages 3-10. **C** and **D**: Graphs illustrating the effect of seeding density and time on growth rate of hRP (**C**) and hREC (**D**) seeded at $5x10^3$, $1x10^4$, $2x10^4$ and $4x10^4$/well in 24w/ps for 21 days. n=3. **E** and **F**: Representative light micrographs of the cells that were used for flow cytometry analysis of surface receptors expressed on hRP P6 (**E**) and hREC P7 (**F**), cultured in healthy conditions until confluent (3-5 days). Results were reported for $1x10^4$ events, % positivity against each fluorophore isotype control. hRP were CD146, CD105 and CD90 positive whilst hREC were CD146, CD31 and CD105 positive. Black scale bars =200µm. **G** and **H**: Immunofluorescence antibody labelling of cell-specific antigens on hRP (**G**), which were Ang-2, Desmin, NG2, PDGFR-β, CD90 and F-actin positive, and hREC (**H**), which were CD31, VE-Cad, ZO-1, vWF, Cx43 and F-actin positive. Isotype controls for normal mouse and rabbit IgG were used as negative controls. Cells were cultured on TC-treated glass until confluent, and imaged using confocal microscopy at x40 oil magnification. White scale bars= 50µm.

Figure 3. Glucose and oxygen analysis for long-term culture of hRP and hREC

hRP (**A**,**B**) and hREC (**C**,**D**) P6 were seeded at $1x10^4$cells/well on 48w/ps in MV +10% FBS or DMEM + 10% FBS, both at 5.5mM glucose. 24H after seeding, cells were transferred to either 20% oxygen or 2% oxygen, FBS was reduced to 5% and glucose was adjusted to 0-35mM for 21 days. Mannitol at 29.5mM + 5.5mM glucose was used as an osmotic control. Resazurin was added at 8 time points in serum-free medium, for 2H. Resazurin media was collected and analysed at excitation 560nm and emission 590nm for n=5/condition, repeated twice. Brown-Forsythe and Welch ANOVA with Dunnett's T3 post-hoc correction was used to determine differences in metabolic activity in 0-35mM glucose and for flow data analysis. For cell number at day 21, DAPI nuclear staining was analysed from 5 fields of view across 5 wells/condition. Unpaired t-test with Welch's correction was used to determine differences between cell counts in 20% or 2% oxygen +

0-35mM glucose at day 21. Data are reported as mean ± standard deviation. *p<0.05, ** p<0.01, ***p<0.001. Scale bar =200µm.

Figure 4. hREC surface antigen expression, barrier properties, angiogenic response and cell size in healthy vs diabetic conditions

A: hREC P5-7 were cultured until confluent (day 0) or for 21 days in either healthy or diabetic conditions to determine any changes to cell surface antigen expression. Results are reported from $1x10^4$ events. The experiment was repeated three times, with one representative run shown here. Brown-Forsythe and Welch ANOVA with Dunnett's T3 post-hoc correction was used to determine differences in surface antigen expression. Black scale bars= 200µm. **B**: Cells were cultured on TC-treated glass for 21 days in 20% or 2% oxygen and 5.5mM or 33mM glucose, in MV +5% FBS. Expression of ZO-1, VE-Cad, CD31, Cx43 and Ang-2 was assessed. Cells were imaged using confocal microscopy at x40 oil magnification. White scale bars =50µm. **C**: cell size (μm^2) from 5 fields of view, across 5 wells/condition, in 3 independent experiments was measured using ImageJ software. Graphs illustrate each measured cell to highlight the spread of cell size in the hypoxic conditions. One-way ANOVA with Holm-Sidak correction was used to determine differences between cell size for each condition, n=3. **D**: Anti-Paxillin antibody was used to determine the number of focal adhesions/cell size (μm^2) in 5 fields of view/well for each condition. *p<0.05, ** p<0.01, ***p<0.001.

Figure 5. Dynamic expression of αSMA, CD146 and CD105 by hRP

A: hRP P5-7 were cultured until confluent (day 0) or for 21 days in either healthy or diabetic conditions to determine any changes to cell surface antigen expression. Results are reported from $1x10^4$ events. The experiment was repeated three times, with one representative run shown here. Brown-Forsythe and Welch ANOVA with Dunnett's T3 post-hoc correction was used to determine differences in surface antigen expression, n=3. There was significant reduction in CD105 at day 21 in healthy conditions vs day 0 (99% ±0.1% vs 55.8% ±11.6%, p=0.0483). Due to large variability in CD146 expression, results were not statistically different. **B**: IF antibody labelling of αSMA on hRP P6 grown for 7 days in healthy conditions on TC-treated glass. Cytoplasmic protrusions from αSMA- positive hREC (green) grown on the underside of the PET appear orange in mono-culture (**C**), co-culture with a confluent hREC apically (**D**), or if hREC did not form a mono-layer apically (**E**). Cells were imaged using confocal microscopy at x40 or x63 oil magnification. Z-stack images were produced using volume view plugin on Image J. Scale bars=50µm.

Figure 6. hREC barrier properties and F-Actin arrangement in mono- & co-culture

A: hREC were cultured on the apical surface of PET transwell inserts for 21 days in healthy or diabetic conditions. **B**: hREC and hRP were co-cultured 1:1, with hRP on the underside and hREC on the apical side of PET transwell inserts. For seeding, treatment and timescale for the models, see Fig. 1b. Antibodies against ZO-1, VE-Cad and Cx43 were used to assess the barrier properties

of the hREC. Phalloidin was used to analyse F-actin arrangement in hREC. Using z-stacking technology and volume view plugin on ImageJ software, hRP were observed on the underside of the PET in the z-projection micrographs. All images were captured using confocal microscopy, x40 oil magnification. Scale bars= 50µm.

Figure 7. Protein secretion profiles of hREC and hRP in healthy vs diabetic conditions
hREC and hRP were cultured on PET membranes at 1:1 ratio, as mono- or co-cultures, in healthy (blue) or diabetic (magenta) conditions, for 21 days. At seven time points media was collected and analysed for secreted Ang-2 (**A-C**), VEGF (**D-F**), PDGF (**G-I**), hHGF (**J-L**), TIMP-2 (**M-O**) and IL-8 (**P-R**), using Quansys Human Angiogenesis Multiplex arrays, with Q-View software. All samples were analysed in technical duplicates, and triplicates for each condition. Results were corrected against a media sample with no cells. Data presented is three independent experiments (n=3), and mean with standard deviation. For VEGF, hHGF and PDGF two independent experiments were analysed due to samples in one repeat being under the lower limit of detection. Two-way ANOVA with Sidak's multiple comparison post-hoc test, to account for repeated measures, was used to perform statistical analysis, using GraphPad Prism 8 software. * $p<0.05$, ** $p<0.01$ and *** $p<0.001$.

Supplementary Figure 1:
hREC P8 were cultured on TC-treated glass slides for 7 days in different O_2 and glucose levels, to induce a diabetic-like phenotype in vitro. Light microscope images were captured at day 7 before fixing, using the Nikon DIAPHOT at x10 magnification. Black scale bars= 200µm. hREC were fixed at day 7 and labelled with antibodies against CD31 and ZO-1 to assess hREC monolayer integrity, Ang-2 to determine angiogenic response, vWF to confirm endothelial phenotype, and SOD-1 to assess oxidative stress response. Slides were imaged using the Zeiss M800 confocal microscope, at x40 oil or x63 magnification. White scale bars= 50µm.

Supplementary Figure 2:
hRP P7 were cultured on TC-treated glass slides for 7 days in different O_2 and glucose levels, to induce a diabetic-like phenotype in vitro. Light microscope images were captured at day 7 before fixing, using the Nikon DIAPHOT at x10 magnification. Black scale bars= 200µm. hRP were fixed at day 7 and labelled with antibodies against NG2 and PDGFR-β to confirm pericyte phenotype, HIF1α to assess hypoxic response and SOD-1 and -2 to determine oxidative stress response. Slides were imaged using the Zeiss M800 confocal microscope, at x40 oil magnification. White scale bars= 50µm.

Supplementary Figure 3:
hREC were cultured on the apical surface of PET transwell inserts for 7 or 14 days in healthy or diabetic conditions. For seeding, treatment and timescale for the models, see Fig. 1b. Antibodies against ZO-1, VE-Cad and Cx43 were used to assess the barrier properties of the hREC. Nuclei

were visualised with DAPI (blue). All images were captured using the Z800 confocal microscope, x40 oil magnification. Scale bars= 50µm.

Supplementary Figure 4:

hREC at P6 and hRP at P7 were seeded as mono- or co-cultures on PET transwell inserts and cultured for 72H until confluent. Cells on inserts were then transferred to either healthy (20% oxygen + 5.5mM glucose) or diabetic (2% oxygen + 33mM glucose) conditions for up to 21 days, as described in Fig.1. Live cells were imaged using the AxioVert A1 at days 7, 14 and 21, to ensure both cell-types were viable in the experimental conditions. Additional images were also captured at day 0, 3, 10 and 17 to validate that cells were present during each sample collection for multiplex analysis (data not shown). Scale bars=200µm.

Supplementary Figure 5:

hRP (**A**) and hREC (**B**), P5 were cultured on PET membranes as mono-cultures, in healthy (blue) or diabetic (magenta) conditions, for 21 days. At seven time points media was collected and analysed for secreted Ang-2, VEGF, PDGF, hHGF, TIMP-2 and IL-8, and using Quansys Human Angiogenesis Multiplex arrays, with Q-View software. All samples were analysed in technical duplicates, and triplicates for each condition. Each experimental repeat is shown as runs 1-3, to highlight variation in magnitude but the similarity in trend in healthy vs diabetic-like conditions. Where graphs are excluded in run 1, protein levels were below the detectable limit.

Supplementary Figure 6:

hREC and hRP, P5 were cultured on PET membranes at 1:1 ratio as co-cultures, in healthy (blue) or diabetic (magenta) conditions, for 21 days. At seven time points media was collected and analysed for secreted Ang-2, PDGF, hHGF, TIMP-2 and IL-8using Quansys Human Angiogenesis Multiplex arrays, with Q-View software. All samples were analysed in technical duplicates, and triplicates for each condition. Each experimental repeat is shown as runs 1-3, to highlight variation in magnitude but the similarity in trend in healthy vs diabetic-like conditions. Where graphs are excluded in run 1, protein levels were below the detectable limit.

Figure 1

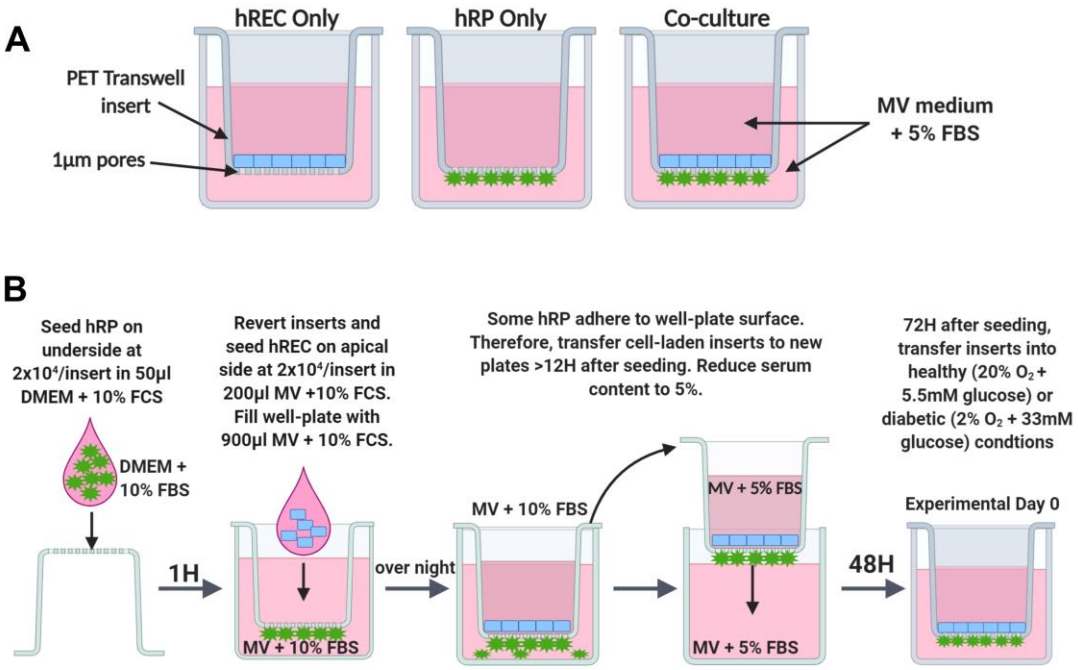
A
hREC Only
hRP Only
Co-culture
PET Transwell insert
1µm pores
MV medium + 5% FBS
B
Seed hRP on underside at 2x10⁴/insert in 50µl DMEM + 10% FCS
DMEM + 10% FBS
1H
Revert inserts and seed hREC on apical side at 2x10⁴/insert in 200µl MV +10% FCS. Fill well-plate with 900µl MV + 10% FCS.
MV + 10% FBS
over night
Some hRP adhere to well-plate surface. Therefore, transfer cell-laden inserts to new plates >12H after seeding. Reduce serum content to 5%.
MV + 10% FBS
MV + 5% FBS
MV + 5% FBS
48H
72H after seeding, transfer inserts into healthy (20% O2 + 5.5mM glucose) or diabetic (2% O2 + 33mM glucose) condtions
Experimental Day 0

Figure 2:

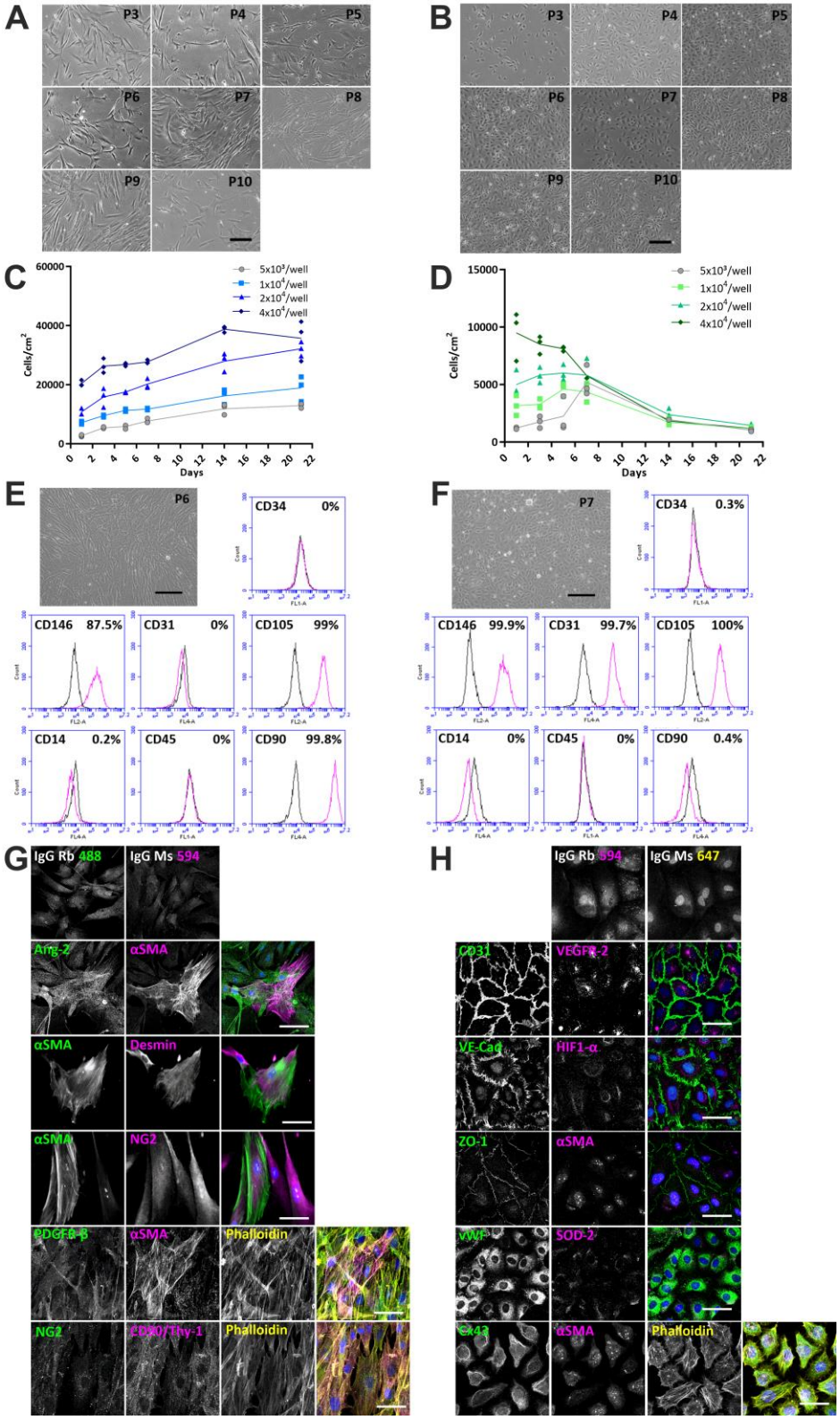
A
P3
P4
P5
P6
P7
P8
P9
P10
B
C
5x10³/well
1x10⁴/well
2x10⁴/well
4x10⁴/well
Cells/cm²
Days
D
E
CD34 0%
CD146 87.5%
CD31 0%
CD105 99%
CD14 0.2%
CD45 0%
CD90 99.8%
F
CD34 0.3%
CD146 99.9%
CD31 99.7%
CD105 100%
CD14 0%
CD45 0%
CD90 0.4%
G
IgG Rb 488
IgG Ms 594
Arg-2
αSMA
Desmin
NG2
PDGFR-β
Phalloidin
CD90/Thy-1
H
IgG Rb 594
IgG Ms 647
CD31
VEGFR-2
VE-Cad
HIF1-α
ZO-1
vWF
SOD-2
Cx43

Figure 3:

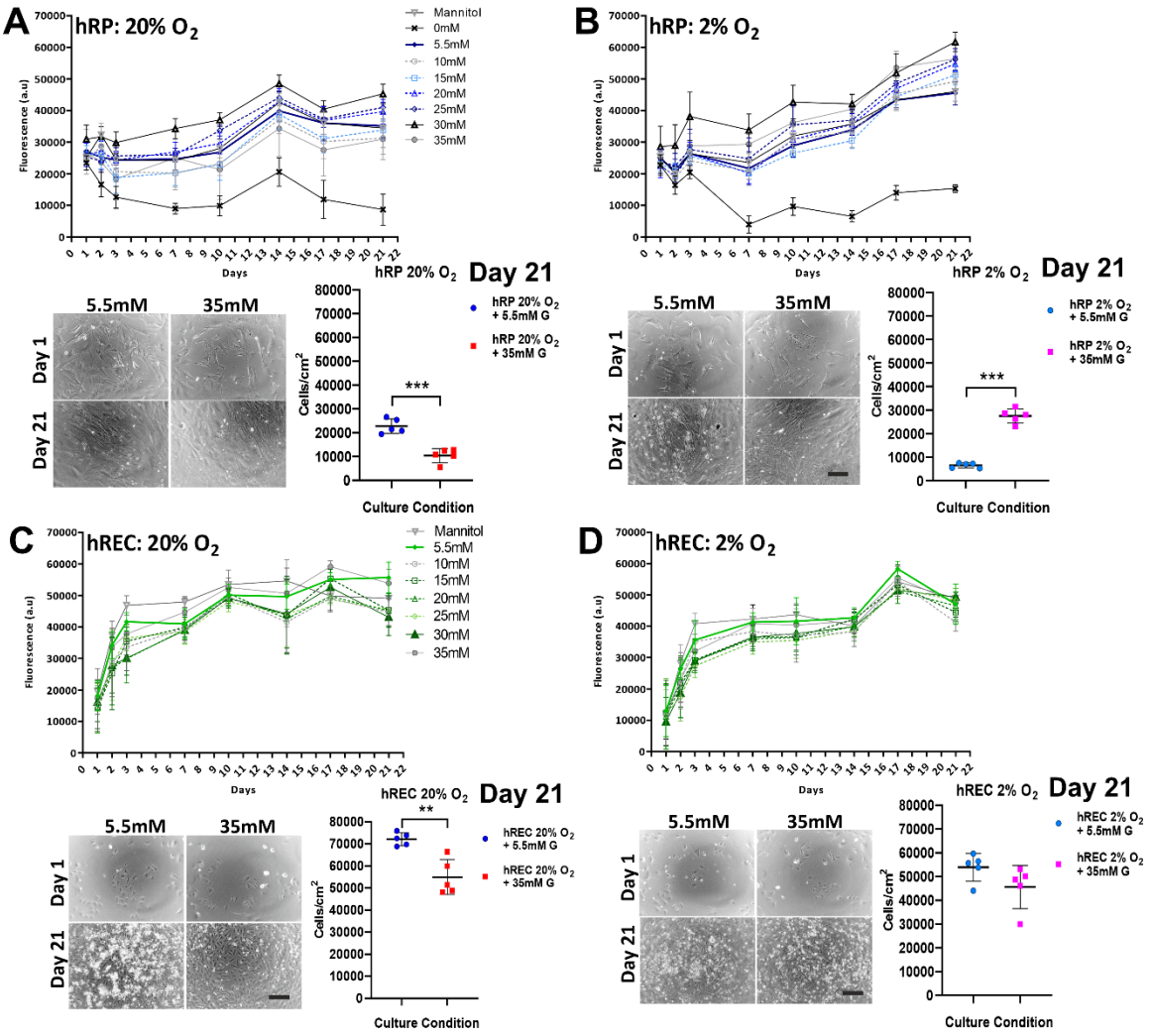
A
hRP: 20% O2
Mannitol
0mM
5.5mM
10mM
15mM
20mM
25mM
30mM
35mM
Fluorescence (a.u)
Days
B
hRP: 2% O2
C
hREC: 20% O2
D
hREC: 2% O2
5.5mM
35mM
Day 1
Day 21
hRP 20% O2 Day 21
hRP 2% O2 Day 21
hREC 20% O2 Day 21
hREC 2% O2 Day 21
hRP 20% O2 + 5.5mM G
hRP 20% O2 + 35mM G
hRP 2% O2 + 5.5mM G
hRP 2% O2 + 35mM G
hREC 20% O2 + 5.5mM G
hREC 20% O2 + 35mM G
hREC 2% O2 + 5.5mM G
hREC 2% O2 + 35mM G
Cells/cm2
Culture Condition
***
**

Figure 4:

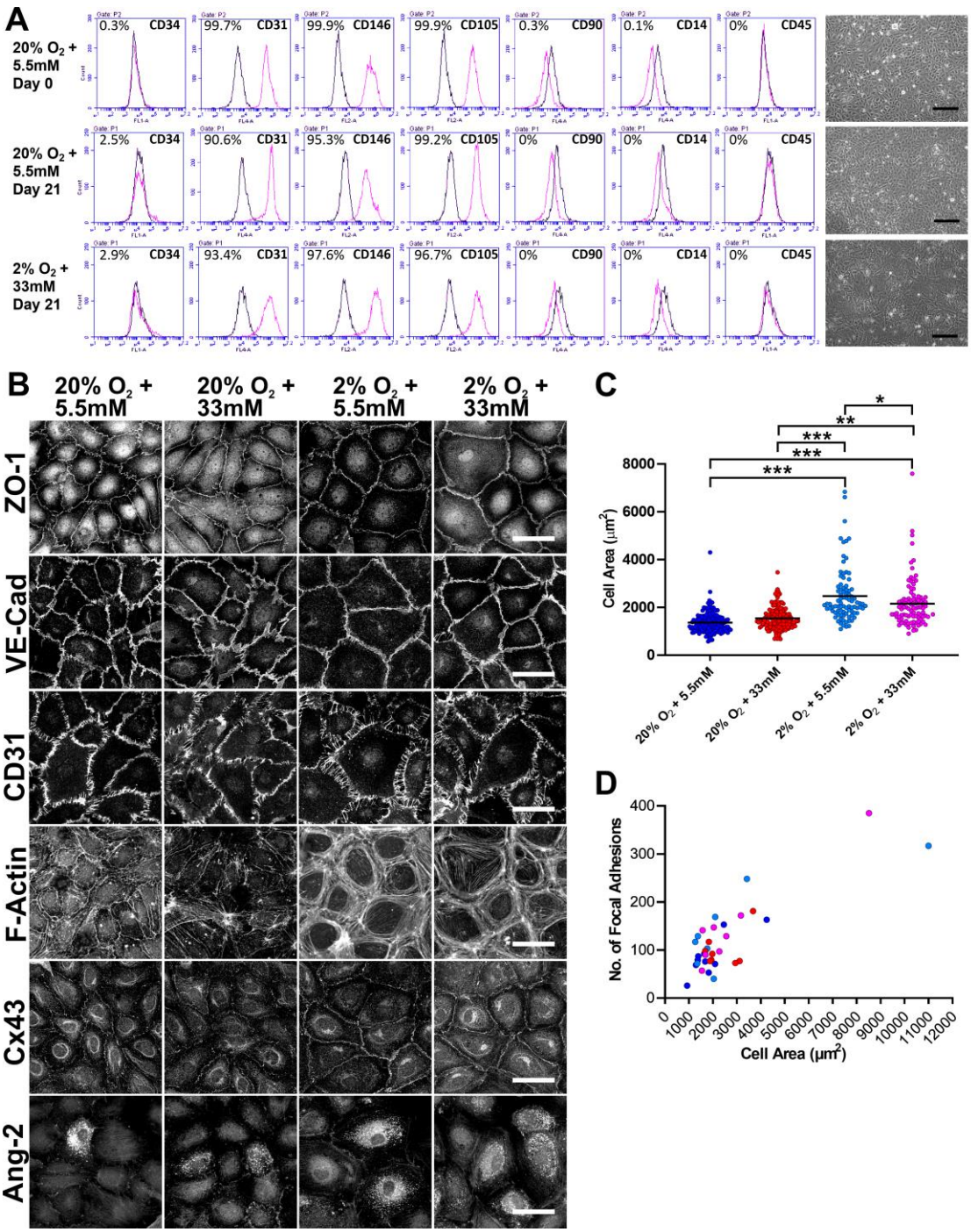
A
20% O2 + 5.5mM Day 0
0.3% CD34
99.7% CD31
99.9% CD146
99.9% CD105
0.3% CD90
0.1% CD14
0% CD45
20% O2 + 5.5mM Day 21
2.5% CD34
90.6% CD31
95.3% CD146
99.2% CD105
0% CD90
0% CD14
0% CD45
2% O2 + 33mM Day 21
2.9% CD34
93.4% CD31
97.6% CD146
96.7% CD105
0% CD90
0% CD14
0% CD45
B
20% O2 + 5.5mM
20% O2 + 33mM
2% O2 + 5.5mM
2% O2 + 33mM
ZO-1
VE-Cad
CD31
F-Actin
Cx43
Ang-2
C
Cell Area (μm2)
8000
6000
4000
2000
0
*
**
***
***
***
20% O2 + 5.5mM
20% O2 + 33mM
2% O2 + 5.5mM
2% O2 + 33mM
D
No. of Focal Adhesions
400
300
200
100
0
0
1000
2000
3000
4000
5000
6000
7000
8000
9000
10000
11000
12000
Cell Area (μm2)

Figure 5:

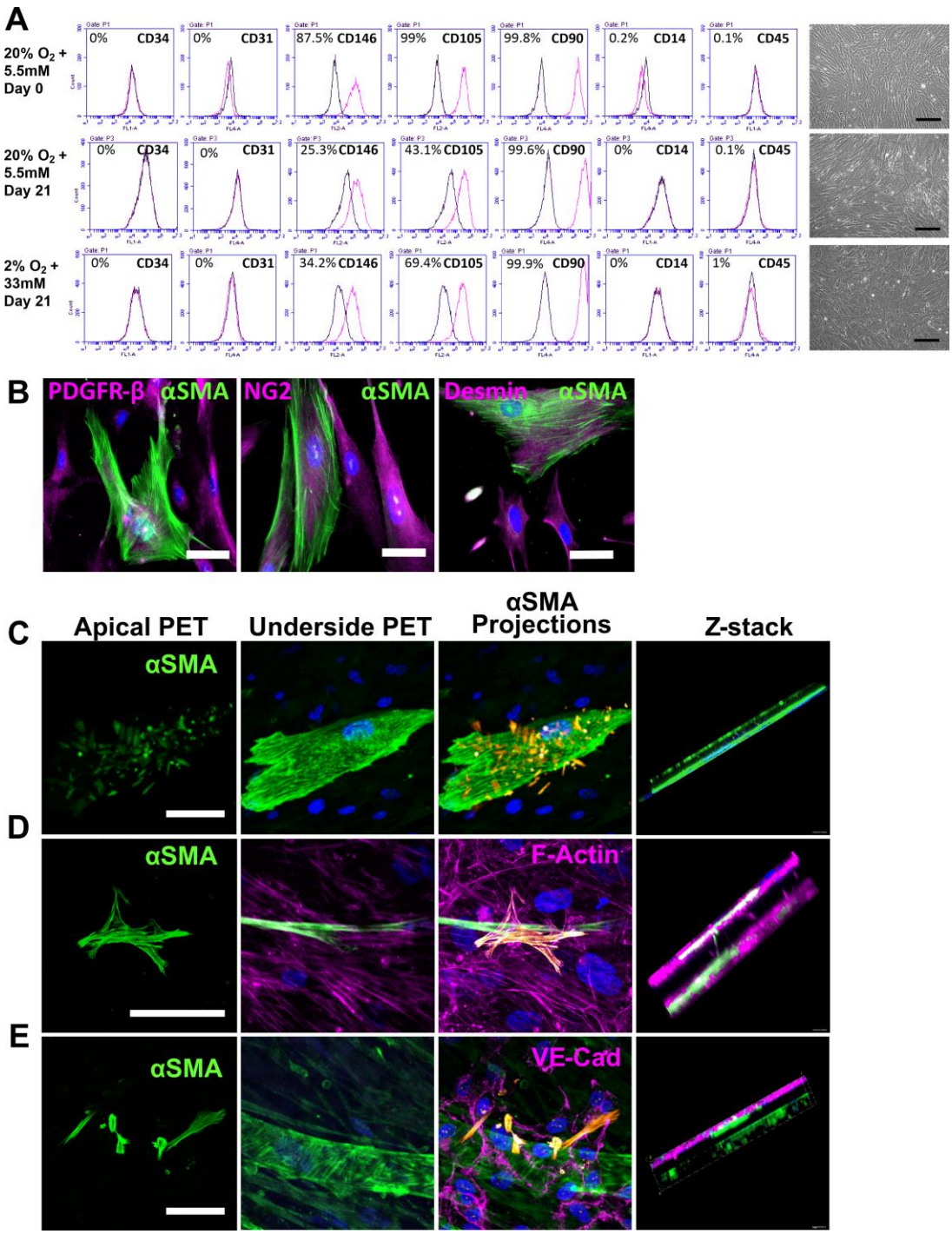
A
20% O2 + 5.5mM Day 0
0% CD34
0% CD31
87.5% CD146
99% CD105
99.8% CD90
0.2% CD14
0.1% CD45
20% O2 + 5.5mM Day 21
0% CD34
0% CD31
25.3% CD146
43.1% CD105
99.6% CD90
0% CD14
0.1% CD45
2% O2 + 33mM Day 21
0% CD34
0% CD31
34.2% CD146
69.4% CD105
99.9% CD90
0% CD14
1% CD45
B
PDGFR-β αSMA
NG2 αSMA
Desmin αSMA
C
Apical PET
Underside PET
αSMA Projections
Z-stack
αSMA
D
αSMA
F-Actin
E
αSMA
VE-Cad

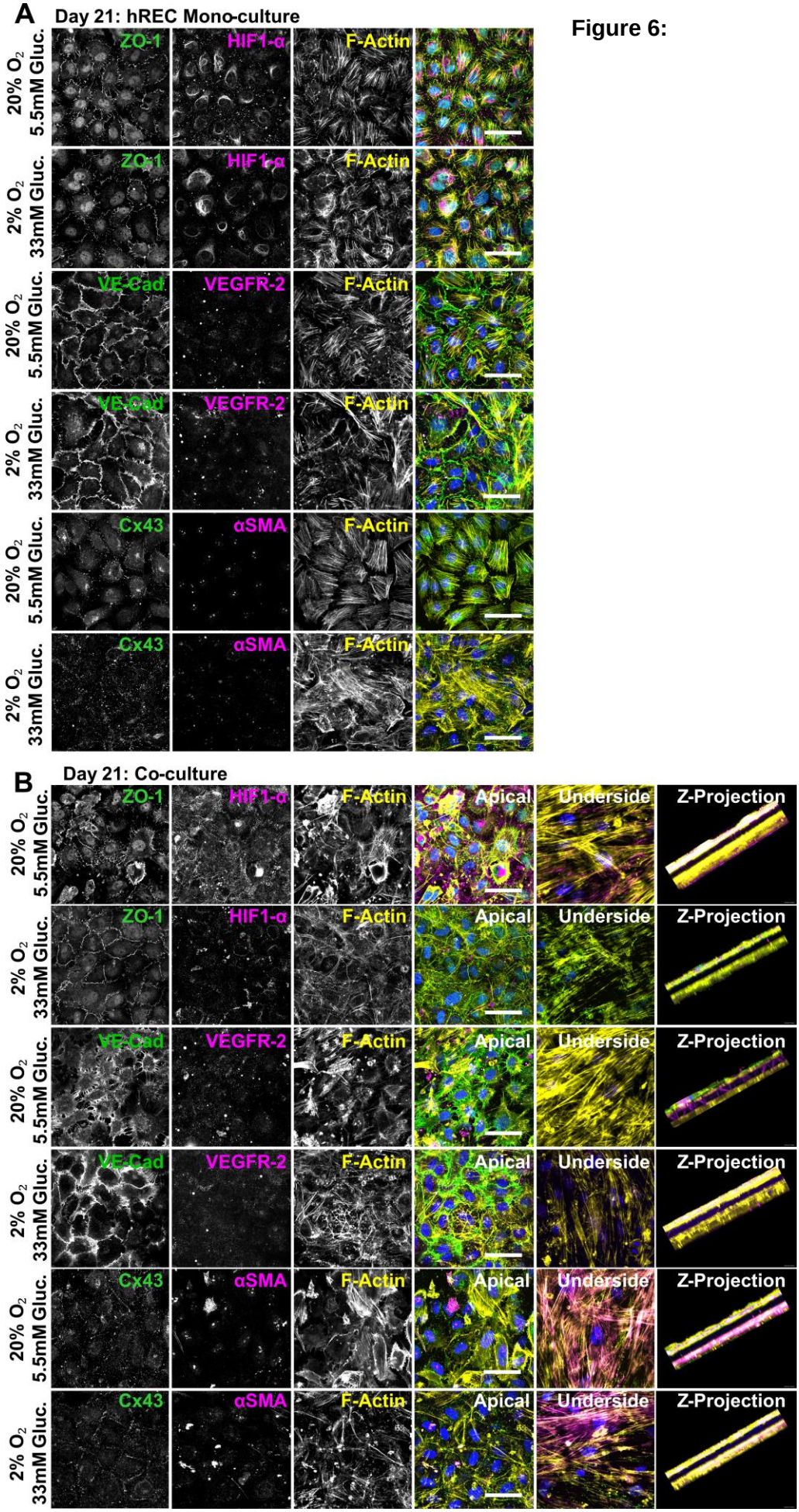
A
Day 21: hREC Mono-culture
20% O2 5.5mM Gluc.
2% O2 33mM Gluc.
ZO-1
HIF1-α
F-Actin
VE-Cad
VEGFR-2
Cx43
αSMA
B
Day 21: Co-culture
Apical
Underside
Z-Projection

Figure 6:

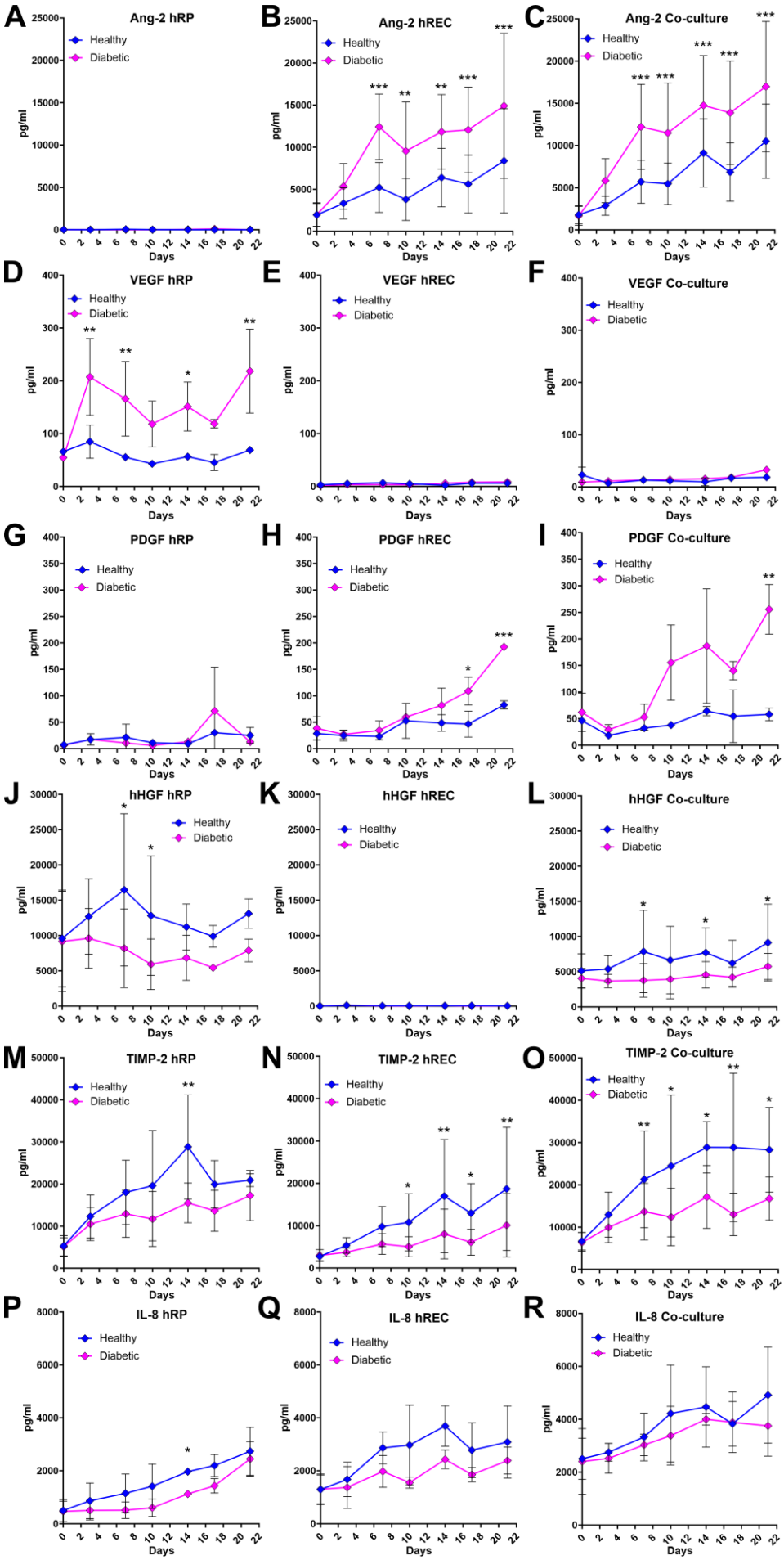
A
Ang-2 hRP
B
Ang-2 hREC
C
Ang-2 Co-culture
D
VEGF hRP
E
VEGF hREC
F
VEGF Co-culture
G
PDGF hRP
H
PDGF hREC
I
PDGF Co-culture
J
hHGF hRP
K
hHGF hREC
L
hHGF Co-culture
M
TIMP-2 hRP
N
TIMP-2 hREC
O
TIMP-2 Co-culture
P
IL-8 hRP
Q
IL-8 hREC
R
IL-8 Co-culture
Healthy
Diabetic
pg/ml
Days

Figure 7:

915

Supplementary 1:

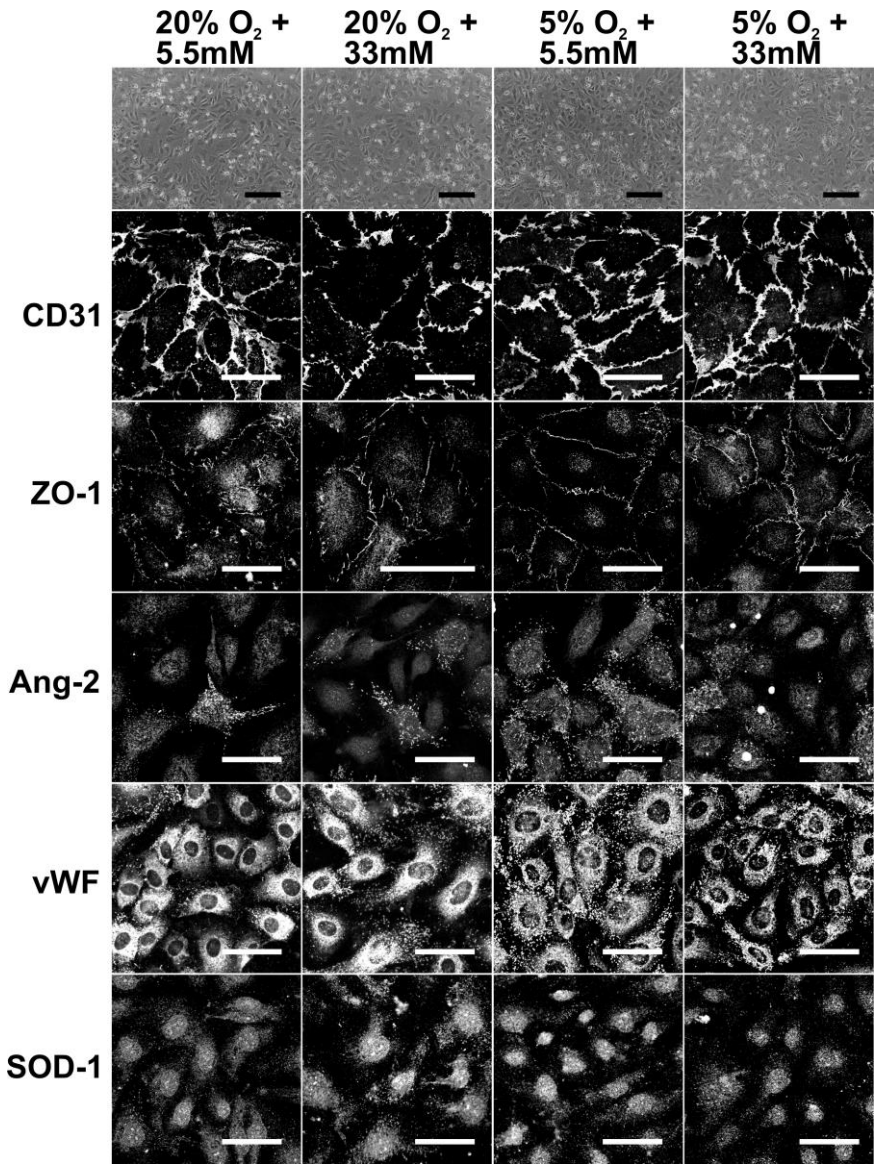

Supplementary 2:

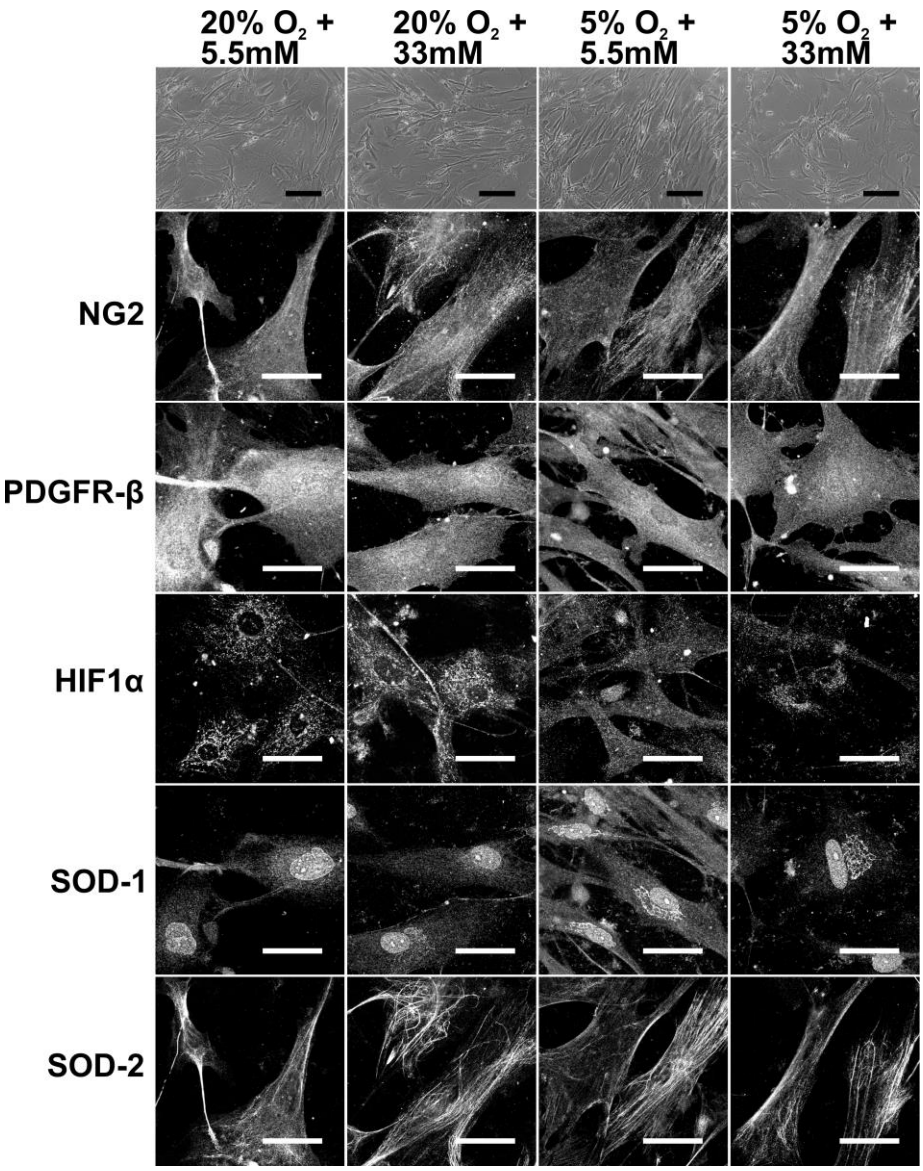

Supplementary 3:

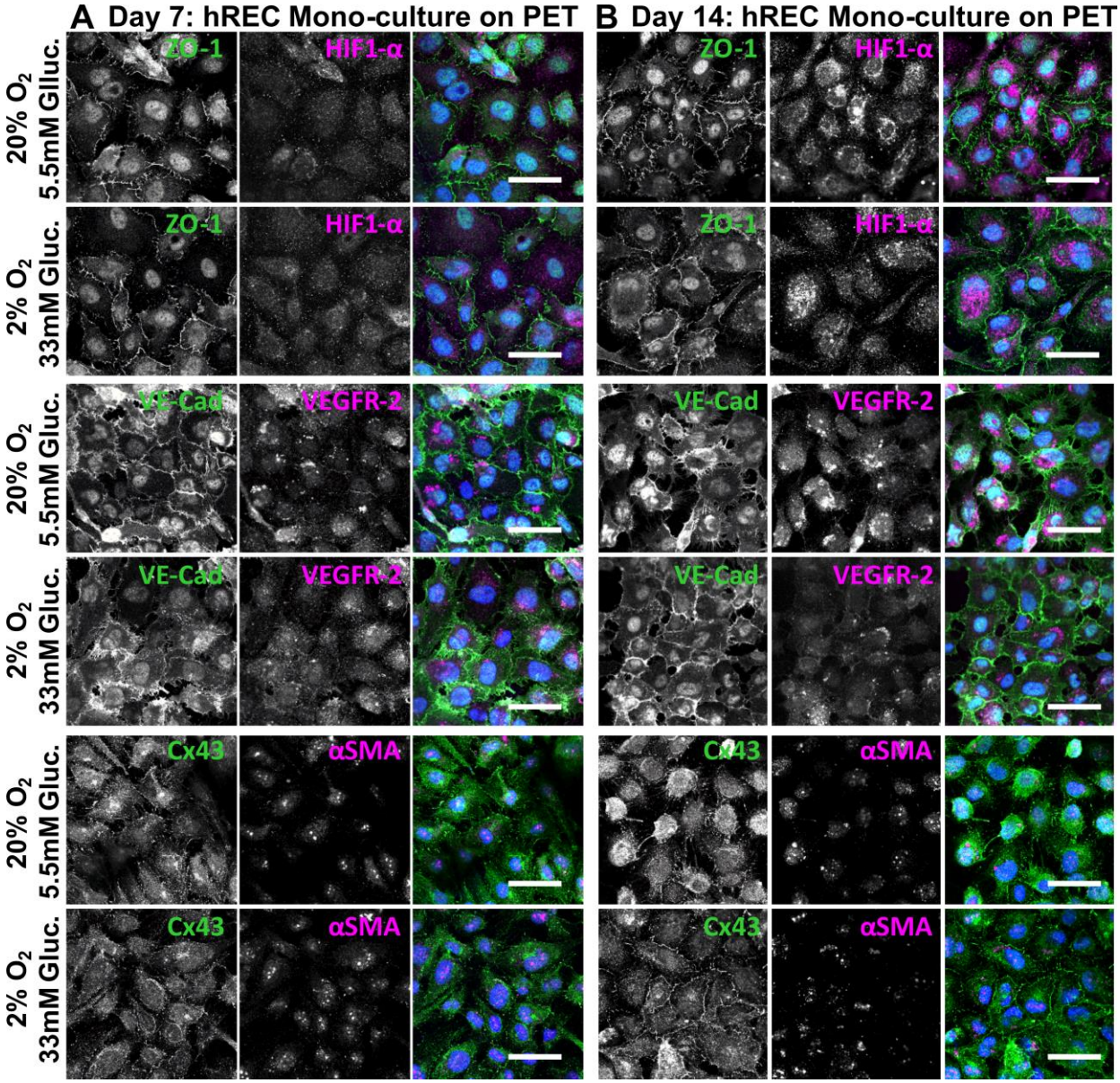

Supplementary 4:

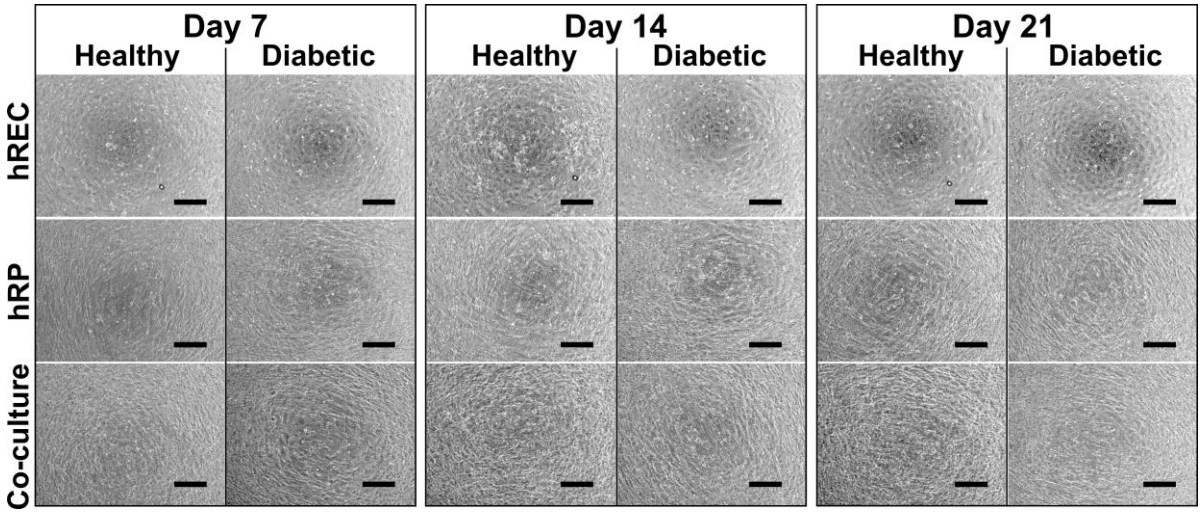

Supplementary 5:

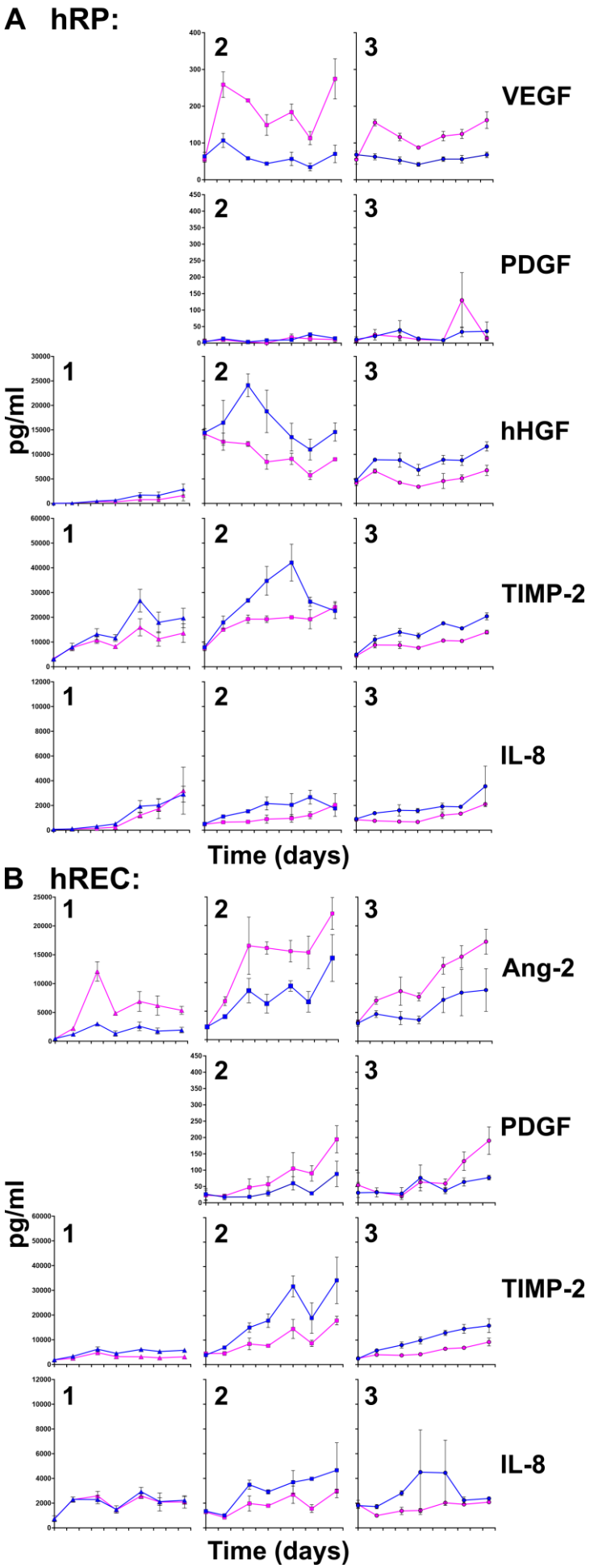

Supplementary 6: